Back-thrusting response of continental collision: Early Cretaceous NW-directed thrusting in the Changle-Nan'ao belt (Southeast China)

Wei Wei, Michel Faure, Yan Chen, Wenbin Ji, Wei Lin, Qingchen Wang, Quanren Yan, Quanlin Hou

Back-thrusting response of continental collision: Early Cretaceous NW-directed thrusting in the Changle-Nan'ao belt (Southeast China)

Wei Wei, Michel Faure, Yan Chen, Wenbin Ji, Wei Lin, Qingchen Wang, Quanren Yan, Quanlin Hou

PII: S1367-9120(15)00026-7
DOI: http://dx.doi.org/10.1016/j.jseaes.2015.01.005
Reference: JAES 2220

To appear in: *Journal of Asian Earth Sciences*

Received Date: 25 August 2014
Revised Date: 24 December 2014
Accepted Date: 9 January 2015

Please cite this article as: Wei, W., Faure, M., Chen, Y., Ji, W., Lin, W., Wang, Q., Yan, Q., Hou, Q., Back-thrusting response of continental collision: Early Cretaceous NW-directed thrusting in the Changle-Nan'ao belt (Southeast China), *Journal of Asian Earth Sciences* (2015), doi: http://dx.doi.org/10.1016/j.jseaes.2015.01.005

Back-thrusting response of continental collision: Early Cretaceous NW-directed thrusting in the Changle-Nan'ao belt (Southeast China)

Wei Wei[a,b,c,d], Michel Faure[b,c], Yan Chen[b,c], Wenbin Ji[b,c,d], Wei Lin[d*], Qingchen Wang[d], Quanren Yan[a], and Quanlin Hou[a].

[a] Key Laboratory of Computational Geodynamics, University of Chinese Academy of Sciences, Beijing 100049, China

[b] Université d'Orléans, ISTO, UMR 7327, 45071 Orléans, France

[c] CNRS/INSU, ISTO, UMR 7327, 45071 Orléans, France

[d] SKL, Institute of Geology and Geophysics, Chinese Academy of Sciences, Beijing 100029, China

[*]Corresponding author: linwei@mail.iggcas.ac.cn

ABSTRACT

The SE coastal area of the South China Block (SCB) is generally interpreted as a Cretaceous active continental margin due to subduction of the Paleo-Pacific plate beneath the Eurasian plate. There, the NE-SW striking Changle-Nan'ao belt was previously considered as a major strike-slip fault zone with a large displacement accommodating the northward subduction of the Paleo-Pacific plate. Our new field and laboratory investigations document a NW-directed ductile thrust zone that placed gneiss upon Early Cretaceous foliated volcanic rocks. Structural analyses and

Anisotropy of Magnetic Susceptibility results indicate that the ductile fabrics in both units are represented by a NE-SW striking foliation and a NW-SE stretching lineation with top-to-the-NW shear sense. This deformation occurred at ca. 130-105 Ma, before the deposition of undeformed (ca. 104 Ma) volcanic rocks, and the intrusion of ca. 90 Ma isotropic plutons. This continent-ward structure is tentatively interpreted as a back-thrust resulting of the collision of the West Philippines microcontinent with the SCB rather than an effect of a simple oceanic subduction.

Keywords: South China Block; East Asia Continental Margin; Changle-Nan'ao belt; Paleo-Pacific Subduction; Cretaceous geodynamics

1. Introduction

During the Late Mesozoic, the East Asia Continent Margin (EACM) experienced an important geodynamic event, featured by i) emplacement of numerous granitic plutons coeval with volcanic rocks in a vast area, ii) the development of a predominant NE-SW striking fault system, and iii) the opening of narrow NE-SW syn-tectonic sedimentary basins (Zhou et al., 2006; Shu et al., 2009; Wang and Shu, 2012; Wang et al., 2013). The geodynamic cause of this Early Cretaceous tectonic-magmatic-sedimentary event is a hot topic in the geosciences community. Noticing that the Late Mesozoic volcanic rocks are characterized by a magmatic arc affinity, many scholars argued that during the Mesozoic time, the EACM was an Andean-type active continental margin related to the subduction of the Paleo-Pacific

plate beneath the East Asia Continent (Jahn, 1974; Lapierre et al., 1997; Li, 2000; Zhou and Li, 2000; Zhou et al., 2006; Li et al., 2012). With the ongoing subduction of the Paleo-Pacific plate, some authors argued that a trail of terranes or microcontinents carried by the oceanic plate was accreted to the East Asia Continental Margin (e.g. Faure et al., 1986; Faure and Natal'in, 1992; Sengör and Natal'in, 1996). In spite of a large amount of geochemical and geochronological data accumulated, the structural aspects, and the tectonic regime related to this major event are still under debate. It was also proposed that the northward oblique subduction of the Paleo-Pacific plate or oblique collision caused by northward drift of Ohkotomorsk block, accommodated by a sinistral strike-slip regime in Eastern Eurasia, was responsible for the activity of the Median Tectonic Line in Japan, Tanlu fault and Changle-Nan'ao Belt (CNB) in China (Xu et al., 1987; Faure et al., 1987; Faure and Natal'in, 1992; Yang, 2013). In this paradigm, the NE-SW trending Cretaceous basins were interpreted as left-lateral pull-aparts (Gilder et al., 1996).

On the contrary to the strike-slip interpretation, Wei et al. (2014a) argued that the paleomagnetic record of the South China Block did not support such a large-distance sinistral displacement. Moreover, on the basis of structural and sedimentological investigations, Shu et al. (2009) considered that most of the Cretaceous NE-SW elongated red bed basins in SCB were half-grabens bounded by a NE-SW striking normal fault on one flank and an unconformity on the other flank. Therefore, the elongation of these basins, as well as their boundary normal fault, suggest a NW-SE extensional regime during sedimentation. This NW-SE tectonic pattern was

interpreted to be formed in a back-arc setting due to the NW-subduction of the Paleo-Pacific slab (Zhou and Li, 2000; Li and Li, 2007; Zhu et al., 2010; Zhu et al., 2012). The records of the contemporary granitoids and ductile shear zones in the South China Block support this NW-SE extensional regime (Faure et al., 2003; Li et al., 2013; Wei et al., 2014b).

Since the Paleo-Pacific slab has totally disappeared, and the subduction direction cannot be directly determined, the geological records from the upper plate, i.e. the East Asian Continental Margin (EACM) are crucial to document the Cretaceous geodynamics of this area. One of the best ways to solve the contradictory interpretations of the Late Mesozoic tectonic regime in the EACM is to study a key area where detailed structural records of this period are still preserved. The CNB is such a key area as it is located on the southeast coast of SCB which is presently the closest place to the assumed Late Mesozoic Paleo-Pacific subduction zone (Fig. 1A; Zhou and Li, 2000 and references therein). Since numerous Mesozoic magmatic and metamorphic rocks, and structures can be observed (Fig. 1B), the CNB attracted many scholars, and it has been differently interpreted. It was first considered as a sinistral intra-continental strike-slip fault, accommodating the Cretaceous deformation owing to the Paleo-Pacific oblique subduction and collision of the West Philippines microcontinent before the Cenozoic opening of the South China Sea (Xu et al., 1987; Faure et al., 1989; Charvet et al., 1990; Zhu et al., 1993). The CNB was also regarded as an oblique collision zone between the SCB and a hypothetic Min-Tai microcontinent with a change of shear sense from sinistral to dextral before the

collision and after the collision respectively (Hsu et al., 1990; Lu et al., 1994; Wang and Lu, 1997). Based on $^{40}Ar/^{39}Ar$ dating, a thrust regime was also proposed to accommodate the exhumation of the high temperature metamorphic rocks exposed in the SE part of the CNB (Chen et al., 2002). Though attractive, this hypothesis needs structural proofs.

Furthermore, the Mesozoic magmatic activity, widespread in the CNB, can provide useful chronological and structural constraints to decipher the Eurasian-Paleo-Pacific relationships. It is well acknowledged that pluton shape and internal fabrics are controlled by the rheological behavior of the magma during its cooling and crystallization (e.g. Van der Molen and Paterson, 1979; Blumenfeld and Bouchez, 1988; Vernon, 1986, 2000; Vernon et al., 1989; Wei et al., 2014b, and enclosed references). Therefore, the characterization of granitic fabric development, namely magmatic, solid-state, or post-solidus state flow provides significant insights on the tectonic evolution of a given area.

As indicated by numerous previous studies, the tree principal axes of the Anisotropy of Magnetic Susceptibility (AMS) ellipsoid, K_1, K_2, K_3 coincide with the three axes of finite strain ellipsoid, X, Y, Z, respectively (e. g. Tarling and Hrouda 1993; Bouchez and Gleizes, 1995; Talbot et al., 2004; Ferre et al., 2014 and references therein). In the magmatic rocks, the AMS fabric is a fast and efficient substitute for the structural fabric when the latter is difficult to acquire.

In this study, structural analysis and AMS measurements of several generations of granitoids, volcanic rocks, and their country rocks have been conducted in order to

answer following questions: 1) What was the Late Mesozoic tectonic regime of the CNB? 2) When did the deformation occur? 3) What is the geodynamic setting of the East Asia Continental Margin?

2. Geological setting of the Changle-Nan'ao belt

2.1 Lithological subdivisions

Located on the SE coast of SCB, in Fujian Province, the CNB is a NE-SW striking, ca. 400 km long and 40-60 km wide, ductile shear zone (Fig. 1A; He and Zhang, 1989; Cui et al., 2013). In agreement with previous workers, particularly Tong and Tobish (1996), we divide the CNB into five lithological and tectonic units (Fig. 1B). 1) The Gneiss Unit consists of foliated granitoids including granodiorite, monzogranite, two-mica granite, and their Late Jurassic (J_3) and Early Cretaceous (K_1) sedimentary country rocks metamorphosed under amphibolite facies condition (Figs. 2A-E). In a few places (near locations 1, 2, 3 and 4 in Fig 1B), metatexite developed at the expense of porphyritic granitoids or paragneiss are observed. Some biotite-amphibolite mafic restites are also preserved within the migmatite. 2) In the northwestern side of the CNB, the J_3 (Douling) and K_1 (Nanyuan) volcanic formations, mainly formed by rhyolite, dacite and andesite was involved in ductile deformation, and experienced a lower green schist facies metamorphism in some places at the same time (Figs. 2F-2H; Tong and Tobisch, 1996). The details will be described below in section 3. In the following, this unit will be referred to as the "Deformed Volcanic Rocks Unit". 3) The magmatically foliated Early Cretaceous syntectonic granitoids

formed mainly by two-mica granite plutons, and also by a minority of gabbro, granodiorite, and monzogranite bodies, intrude into the above two deformed units (Fig. 2I). This unit was not emphasized by many former authors due to the poorly expressed macroscopic fabric, however as documented below by microstructural analyses, we argue that these plutons experienced a deformation developed in a magmatic stage during the granitic magma crystallization. In the following, this unit will be referred to as the "syntectonic granitoids" unit. 4) Late Cretaceous undeformed isotropic plutons of monzogranite, alkaline granite, syenite, two-mica granite, mostly with alkaline geochemical affinity, and NE-SW dykes intruded into the previous rocks (Fig. 2J). NE-SW striking late narrow shear zones cross cut these granites (Fig. 2K). 5) The Late Cretaceous undeformed volcanic rocks of the Shimaoshan formation unconformably cover the deformed rocks (Fig. 2L; Guo et al., 2012).

2.2. Bulk architecture of the CNB

Underlying the Late Cretaceous unconformity of the Shimaoshan volcanic formation, and cross-cut by undeformed Late Cretaceous plutons, the Early Cretaceous volcanic rocks, the Early Cretaceous volcanic rocks and the Triassic-Jurassic sedimentary rocks are involved in NE-SW striking, upright or NW-verging, folds. Two ductile shear zones deform this kilometer thick volcanic-sedimentary sequence (Figs 3 and 4), however, due to poor outcrop conditions, the existence of additional shear zones cannot be discarded. Along these NE-SW striking ductile shear zones, the Early Cretaceous volcanic rocks are pervasively foliated and lineated. These structures are analyzed in detail in section 3,

below. In the Gneiss Unit also, the foliation was overprinted by km-scale, NE-SW striking upright antiforms and synforms. As a whole, the well-foliated Gneiss Unit is at a high angle fault contact with the J_3-K_1 Deformed Volcanic Rocks Unit. Although the direct contact between the two units is not observed in the field, a regional thrust of the Gneiss Unit upon the Deformed Volcanic Rocks Unit is depicted in the interpretative cross sections (Fig. 4), as discussed in section 6.

2.3. Geochronological constraints

In the past decades, hundreds of radiometric dating data have been performed in the CNB. This geochronological dataset shows that the ^{40}Ar-^{39}Ar ages of the deformed rocks range from 133 Ma to 84 Ma (Wang and Lu, 2000; Chen et al., 2002). U-Pb zircon dating indicates that the gneissic granitoids are older than 130 Ma, while the isotropic granitoids are younger than 100 Ma. Most of the isotropic alkaline plutons of unit 4 emplaced at ca. 90 Ma are interpreted as intraplate bodies (Li et al., 2014). The ages of the granitoids, which are interpreted as the syntectonic granitoids of unit 3 are in the 130-105 Ma interval (Tong and Tobisch, 1996; Li et al., 2003; Liu et al., 2012; Cui et al., 2013). The details of these syn-tectonic granitoids are provided in section 3. The NE-SW striking dykes yield a ca. 90 Ma age (Dong et al., 2006). The ductilely deformed volcanic rocks erupted from 168 to 130 Ma, whilst the undeformed ones erupted during the 104-95 Ma interval (Guo et al., 2012). It is worth to note that a volcanic quiescence, which corresponds to the time of the main ductile deformation presented below, occurred between 130 Ma and 104 Ma (Guo et al., 2012).

3. New structural insights

In order to achieve a general picture on the deformation pattern of the CNB, and to decipher its tectonic evolution, we conducted a systematic structural investigation with special attention paid to the various granitic rock-types. For the outcrops where only the foliation was observable in the field, an AMS study following Borradaile and Henry (1997) methodology has been carried out to assess the magnetic foliation, and determine the magnetic lineation. Our field structural observation and lab AMS measurement enable us to recognize the bulk geometry of the CNB and to distinguish three tectonic events that occurred in the CNB, namely E_1, E_2 and E_3, respectively. The E_1 event was well recorded in the Gneiss Unit and the Deformed Volcanic Rocks Unit, the E_2 event was featured by the emplacement of dykes and undeformed isotropic granitoids, and the E_3 event was characterized by the narrow local shear zone which cross cut the previous rocks. The detail of our AMS study is provided in section 4. Here, we depict the main macroscopic structural elements at the outcrop and regional scales.

3.1 Gneiss Unit

A pervasive ductile deformation is recognized in the Early Cretaceous granitoids, now transformed into (augen) orthogneiss, and their micaschist country rocks (Figs. 2A-E, 3 and 4). The foliation, consisting of ductilely deformed quartz grains and oriented micas and feldspar, is predominantly striking NE-SW with variable dip angles (Figs. 2A, 3 and 5A; Appendix 1 and 2). NW-verging, meter-scale folds with

NE-SW striking axes are widely observed (Figs. 2B, 3 and 5A). A mineral and stretching lineation, marked by elongated quartz grains, feldspar porphyroclasts, mica aggregates and deformed enclaves is scattered (Fig. 5C). When the foliation is weakly or moderately inclined, the lineation dominantly trends NW-SE; when the foliation is steeply inclined, the lineation is down dip or weakly inclined to the NE-SW. Most of this NE-SW sub horizontal lineation occurs in Dongshan Island (location 1 in Fig. 3).

Field observations of sigmoidal quartz (Fig. 2C), K-feldspar porphyroclast indicate a top-to-the-NW shear sense when the lineation is NW-SE trending with a small dip angle. When the foliation is steep, and lineation is down dip, the kinematic indicators show that the SE side is moving upwards, and correlatively, the NW side, downward. No shear sense can be established along the NE-SW horizontal lineation. In the metamorphic rocks of the Gneiss Unit, the mineral lineation is represented by consistently well-oriented amphibole needles, mica flakes, and quartz rods. These minerals indicate that the deformation occurred under amphibolite facies metamorphic conditions (Fig. 2D). The occurrence of metatexites in the Gneiss Unit (for instance near locations 1, 2, 3 and 4 in Fig. 1B) with oriented biotite and quartz-feldspar leucosomes also argues for high temperature conditions during this tectonic event (Fig. 2E).

3.2 Deformed Volcanic Rocks Unit

The J_3 and K_1 lavas of the Deformed Volcanic Rocks Unit share the same planar and linear fabrics as the Gneiss Unit. However, contrary to the pervasively developed foliation in the Gneiss Unit, the ductile deformation in the Deformed Volcanic Rocks

Unit is heterogeneous, and localized along several mylonitic shear zones. In between the shear zones, the volcanic rocks were not deformed (Figs. 2F-2H, 3, 4A-4D and 5A-5D). Field observations of shear bands and sigmoidal quartz aggregates indicate a top-to-the-NW sense of shear when the lineation is dipping at a shallow angle. When the lineation is steeply dipping, SE-side-moving up/NW-side-moving down shear sense is recognized (Fig. 2G and 2H). The asymmetric folding of the foliation indicates a NW vergence of the post-folial folds that complies with the ductile syn-folial kinematics. In the Jiangyin island (location 7 in Fig. 3), the bedding-cleavage relationships in the sediments intercalated in the volcanic rocks comply with the NW-verging folds.

The exact boundary between the Gneiss and the Deformed Volcanic Rocks Units is not exposed, however, in the Fuqing area, in the Deformed Volcanic Rocks Unit near the contact, a vertical ultramylonitic zone striking N55E with down dip lineation, shear bands, and asymmetric folds are observed indicating a SE-side-moving up/NW-side-moving down shear sense (Fig. 2G and 2H; near location 8 in Fig. 3). Furthermore, on the Gneiss Unit side of this boundary, the orthogneiss foliation strikes N70E and dips NW85 (near location 8 in Fig. 3). Along the down dip stretching lineation, asymmetric tails around K-feldspar indicate a SE-side-moving up/NW side-moving-downward sense of shear (near location 8 in Fig. 3).

3.3 Syntectonic granitoids

In the CNB, most of the syntectonic granitoids consist of an undeformed core and a magmatically foliated rim defined by the preferred orientation of biotite,

feldspar and amphibole without macroscopic deformation features in the outcrop scale (Figs. 2I and 3). The mafic enclaves included in these syntectonic granitoids are parallel to the magmatic foliation of the host rocks without exhibiting a post-solidus deformation (Li et al., 2003). On the southeast coast of the Dongshan island (location 1 in Fig. 3), the margin of a two-mica granite pluton is oriented in accordance with the micaschist country rock foliation, while inside the massif, the preferred orientation is poorly developed, only represented by NE-SW striking schlierens without post-solidus deformation features. The similar trend of schlieren, mineral magmatic fabric and metamorphic foliation of the country rock argue for a contemporary magma intrusion with the regional deformation, thus represents a syntectonic pluton. Although no age has been acquired for this syntectonic pluton, in the central part of the Dongshan Island, another pluton, which was also considered as syntectonic pluton has been dated at 122 Ma by zircon U-Pb dating (Tong and Tobisch, 1996). Near Duxun (near location 4 in Fig. 3), a two-mica granite yielding a 120 Ma age (Cui et al., 2013) exposes an isotropic core and a foliated rim oriented N65E, SE55. On the coast of Weitou and Niutouwei (locations 5 and 9 in Fig. 3), augen granodiorites are dated at 108 Ma and 130 Ma, respectively (Liu et al., 2012), representing deformed rims of syn-tectonic plutons with their main parts covered by sea. In the Gaoshan area, the mafic microgranitoid enclaves included in these plutons are oblate and parallel to the NE-SW striking magmatic foliation (near location 9 in Fig. 3). In the Hui’an and Putian area, pluton featured by a NE-SW magmatic foliation without post-solidus deformation (near location 6 in Fig. 3) was dated at 130 Ma (Li et al., 2003).

3.4 Isotropic Granitoids and Undeformed Volcanic Rocks

Undeformed isotropic plutons (Fig. 2J), younger than 100 Ma, intruded the CNB without altering the previous country rock fabric (e.g. location 2 in Fig. 3). The volcanic activity, coeval with these isotropic granitoids, is represented by undeformed lava flows of the Late Cretaceous Shimaoshan Formation (Figs. 1B and 2L). However, the dykes intruding the previously deformed rocks, and even the undeformed granites, predominantly strike NE-SW and dip at a high angle (Figs. 1B and 5A). This geometric feature argues for a regional NW-SE moderate stretching. Furthermore, no horizontal shearing can be associated with the emplacement of these dykes that appears as pure extension fractures.

3.5 Late narrow strike-slip shear zones

NE-SW strike-slip shear zones crop out in few sites in our study area. These shear zones of only a few centimeters to meters in width received already a great attention (Tong and Tobisch, 1996; Wang and Lu, 2000). However, though mylonitic and ultramylonitic fabrics develop there, they are distinct from the pervasive structures described above in the Gneiss and the Deformed Volcanic Rocks Units. In outcrops, quartz grains were severely stretched to form ribbons or deformed into a "sigmoidal" shape indicating a dextral strike-slip motion. Such narrow strike-slip shear zones crosscut the pervasively deformed rocks (Wang and Lu, 2000), syn-tectonic granitoids (location 4 in Fig. 3) and undeformed isotropic granitoids (Fig. 2K, location 9 in Fig. 3) indicating a late deformation event in the CNB evolution.

3.6 The polyphase deformation in the CNB

In summary, the structural pattern of the CNB is characterized by a polyphase solid-state ductile deformation in the Gneiss Unit and Deformed Volcanic Rocks Unit. The syn-tectonic granitoids exhibiting a sub-solidus magmatic flow, the Late Cretaceous isotropic undeformed granitoids intruding previous rocks, and the undeformed volcanic rocks unconformably covering the previously foliated rocks provide a time constraint (Figs. 4A-4D).

The deformation structures described in this section, allow us to recognize three main deformation events, namely from the older to the younger, E_1, E_2, and E_3. The E_1 event is further subdivided into E_{1a} and E_{1b} sub-events in terms of structural superimposition, however, as they present a kinematic continuity the E_{1b} sub-event is considered as a late increment of the E_1 event.

The E_{1a} sub-event that controls the main structures of the CNB is responsible for the formation of an initially weakly inclined foliation, S_1, and a NW-SE striking mineral and stretching lineation, L_1, with a top-to-the-NW shearing (Figs. 3 and 5). In spite of a consistent strike of the foliation, the lineation scatters both in strike and dip (Figs. 5A-5D). Here, we argue that the two groups of L_1, namely, the one whose direction is perpendicular to the strike of the foliation, and the one whose direction is parallel to the strike of the foliation. The dispersion of L_1 is due to the E_{1b} event that folded the S_1 foliation, and rotated the NW-SE L_1. In order to define the original orientation of the lineation, it is necessary to restore S_1 to its initial weakly inclined geometry. For simplicity, we corrected the foliation to a uniform flat-lying attitude, though the initial geometry of the S_1 foliation might have been slightly inclined as

well. Thus after restoring S_1, to a sub-horizontal attitude, most of the L_1 mineral lineations concentrate along the NW-SE direction, except for a few number of the NE-SW horizontal ones (Fig. 5E and 5F). Representing 25% of the total amount of the measured lineation, the NE-SW lineation is mostly exposed in the Dongshan island (location 1 in Fig. 3). In the SE part of this area, in Aojiao and Sufeng villages, a NE-SW mineral lineation, parallel to the axes of NW-verging recumbent folds is observed (Fig. 2B, location 1 in Fig. 3). The kinematic significance of the NE-SW lineation will be discussed after the micro structural analysis presented in section 5.

The E_{1b} event, responsible for the folding of S_1 in the Gneiss and Deformed Volcanic Rocks Units, produced an important variation in dip of both foliation and lineation. The NW vergence of the folds is consistent with the E_{1a} kinematics (Figs. 5A-5D).

The E_2 event is coeval with the opening of NE-SW striking brittle cracks, some of which were filled by dykes (e.g. Dong et al., 2006). These NE-SW striking dykes with similar age can be easily traced along the coast area of South China (Zhou et al., 2006; Dong et al., 2010).

The E_3 event is represented by the late NE-SW narrow shear zones. Although the regional tectonic bearings and deformation age remain unknown, as they are younger than the undeformed isotropic pluton in which they intrude, a Cenozoic age might be proposed. The discussion on this E_3 event is beyond the scope of this study, in the following, these structures will not be considered.

4. Rock Magnetism Study

4.1 Sampling and experiments

The anisotropy magnetic susceptibility (AMS) is an effective method to determine fabrics in weakly deformed rocks (Tarling and Hrouda, 1993). Owing to the weak deformation developed in many places of the CNB, only foliation was sometimes observable in the field. In order to assess the lineation strike, oriented hand samples of deformed volcanic rocks and orthogneiss from 15 sites were cut into 2cm×2cm×2cm standard cubic specimens to conduct the AMS measurement in the lab. Besides, AMS sampling has been carried out by gasoline driller on pervasively post solidus deformed granitoids in 12 sites (Table 1). Globally, the sites are distant at least 2 km from each other. In each sites, 5-6 AMS standard cores with 2.5 cm in diameter were drilled. All the AMS sampling were conducted in the sites in which only monocline of foliation developed in the outcrop scale and free of any late narrow shear zone cross cutting the foliation. Each core was oriented by both magnetic and solar compasses when possible. In the lab, all cores were cut into standard cylinder specimen with 2.2 cm high. Totally, 116 standard cubic and 95 standard cylinder specimens were prepared.

In Laboratoire de Magnétisme des Roches d'Orléans, IRM experiments were carried out on different lithologies by IM30 pulse magnetizer and JR5 magnetometer. Coupled with a CS3 furnace, KLY3 was used to perform the thermal-susceptibility experiments on powders of different lithologies. The KLY3 kapabridge was also used to perform the AMS and bulk susceptibility measurements. The results were

processed by ANISOFT (offered by AGICO) to calculate the main magnetic anisotropic axes (K_1 for lineation and K_3 for the pole of foliation), the shape parameter (T) and the anisotropy degree (P_J). Moreover, hysteresis curves were obtained by AGM and VSM electromagnetic inductometer on different lithologies in the Paleomagnetic Laboratory of Institut de Physique du Globe de Paris. The Micromag VSM software has been used to process the hysteresis loop data.

4.2 Magnetic mineralogy

The types and size of the magnetic minerals determine the AMS ellipsoid which often corresponds to the strain ellipsoid (cf. Tarling and Hrouda, 1993; and Borradaile and Henry, 1997 for details). In the normal situation, the magnetic carriers are paramagnetic mineral or multi-domain magnetite, then the K_1 and K_3 axes of the magnetic ellipsoid of a measured specimen represent the maximum and minimum axes of the finite strain ellipsoid, respectively. On the contrary to normal situation, the K_1 and K_3 of the magnetic ellipsoid of the anti-paramagnetic mineral and the single domain of the magnetite represent the minimum and the maximum axes of the strain ellipsoid, respectively (Tarling and Hrouda, 1993; Borradaile and Henry, 1997). In order to reach a correct interpretation of AMS mode, it is necessary to determine the magnetic susceptibility carrier.

The measurements show that the bulk susceptibility of most of volcanic rock specimens is usually weak, ranging from 1×10^{-4}SI to 1×10^{-3}SI, few specimens with higher values could reach 4×10^{-3}SI (Table 1; Fig. 6). The bulk susceptibilities of the migmatite and pervasively sub-solidus deformed granitoids show high values, ranging

from 1×10^{-3} to 30×10^{-3} SI (Table 1 and Fig. 6).

Thermal-susceptibility curves indicate that at the temperature of 580°C, the susceptibilities of the migmatite and pervasively sub-solidus deformed granitoids drastically decrease (Fig. 7A and 7B), indicating that magnetite is present in these rocks. In some specimens, the susceptibilities continue to decrease after 580°C indicating the existence of hematite. The thermal-susceptibility curves of the majority of deformed volcanic rocks specimens show that the susceptibilities decrease slowly with the increasing temperature without an apparent rapid drop. Considering the low susceptibility value of this kind of specimens, a paramagnetic mineral is considered as the main magnetic carrier (Fig. 7C). In some specimens of the deformed volcanic rocks, although the susceptibilities are very low, the thermal-susceptibility rapidly decreases at 580°C indicating the existence of a low concentration of magnetite.

The shapes of hysteresis loops of migmatite and pervasively sub-solidus deformed granitoids, featured by a sigmoidal shape, indicate that the main magnetic susceptibility carrier is magnetite (Fig. 7D and 7E). In the hysteresis loops of deformed volcanic rocks, the induced magnetization varies in proportion to applied magnetic field without any saturation (eg. Fig. 7F and 7I). The hysteresis loop of some specimens shows a mélange of a main linear shape with a small fraction of sigmoidal shape (Fig. 7F). The shapes of the hysteresis loops of deformed volcanic rocks indicate that the main magnetic susceptibility carriers are paramagnetic minerals such as biotite and, in some individual specimens, a small amount of magnetite.

IRM curves show that in the applied magnetic field under 100mT, the induced

remnant magnetization rapidly increases and almost attends the saturation (Fig. 7G and 7H) indicating that the predominant magnetic carriers are magnetite in migmatite and pervasively sub-solidus deformed granitoids.

In the Day-plot diagram (Dunlop, 2002), the magnetite sizes reveal that the pseudo-single domain magnetite predominates in the migmatite, pervasively sub-solidus deformed granitoids and deformed volcanic rocks (Fig. 8).

In summary, for the deformed volcanic rocks, the main magnetic carriers in most of the samples are paramagnetic minerals, while pseudo-single domain magnetite is for trivial samples. The pseudo-single domain magnetite can be considered as the main magnetic susceptibility carriers for the migmatite and pervasively sub-solidus deformed granitoid. Therefore, in this study, the magnetic fabrics in the majority of lithologies can be directly correlated with magmatic or tectonic fabrics (e.g. Tarling and Hrouda, 1993).

4.3 AMS results

The AMS data of the CNB are listed in Table 1. The statistics of K_1 and K_3 distributions (Jelinek, 1981) show that the principal axes of AMS are relatively well grouped with the maximum and minimum confidence angles (α_{95max} and α_{95min}) lower than 20°, indicating that the AMS data are significant to be used in the structural interpretation.

In the Km-P_J diagram (Fig. 9A), The P_J values of pervasively sub-solidus deformed granitoids are mostly above 1.2, while the P_J values of deformed volcanic rocks are mostly lower than 1.2 indicating that the deformation degree of pervasively

sub-solidus deformed granitoids is higher than deformed volcanic rocks. In the P_J-T diagram (Fig. 9B), most of the positive T values indicate an oblate shape for the AMS ellipsoid.

The measured magnetic foliation shows a good consistency with the field structural observation (Table 1 and Appendix 1). In several sites where both structural and magnetic lineations are available, the magnetic lineation is also consistent with the structural lineation (Table 1 and Appendix 1). According to our magnetic mineralogical investigation, we used the magnetic lineation as a proxy of the structural lineation in the localities where the latter was not available. Plotting the magnetic fabric in the same stereographic projection diagram of the structural fabric, the similar trend is obvious between two kinds of fabrics (Figs. 5A-5D). The tectonic significance of the AMS measurements will be presented in the "Discussion" section.

5. Microscopic observation and kinematics

In order to define the deformation style and assess the shear sense of the deformed rocks, oriented thin-sections, cut parallel to the structural/magnetic lineation, and perpendicular to the structural/magnetic foliation (XZ section), have been prepared either from oriented hand specimens sampled in the field, or from the AMS cubic or cylinder standard specimens. Besides, for the specimens in which a NE-SW shallowly inclined lineation developed, oriented thin-sections perpendicular to the structural/magnetic lineation, and perpendicular to the structural/magnetic foliation, i.e. in the YZ section, were also prepared in order to determine the maximum

stretching direction.

The deformation structures of pervasively sub-solidus deformed granitoids and micaschist of the Gneiss Unit are described in agreement with classical microstructural analysis (e.g. Passchier and Trouw, 2005; Vernon 2000 and enclosed references). In the thin-sections oriented in the XZ plane, made from the specimens with a NW-SE or highly inclined lineation, feldspars and micas are conspicuously elongated (Fig. 10A). The quartz grains are stretched; even some experienced a dynamic recrystallization with neograins exhibiting an oblique grain shape foliation (Fig. 10B). Moreover, oblique or sigmoidal shapes with bent strings of inclusions also argue for a non-coaxial strain regime (Fig. 10C), which indicate a post-solidus ductile deformation (Paterson et al., 1989; Passchier and Trouw, 2005). In the case of low angle structural/magnetic foliation, the shear sense is top-to-the-NW, while when the foliation is highly dipping to the SE, the sense of shear indicates the SE-side-moving up and NW-side-moving down. In XZ thin-sections made from the specimens with NE-SW striking low angle structural/magnetic lineation, the micas are well oriented, and quartz grains with wavy extinction are moderately stretched, but incipient recrystallization develops sub-grains elongated parallel to the foliation. Moreover, no shear sense has been observed along the NE-SW structural/magnetic lineation in such thin-section. In the YZ thin-sections of such specimens, shortening as indicated by folds and kinked micas can be documented (Fig. 10D).

In the oriented thin-sections made from deformed volcanic rocks, along the direction parallel to the NW-SE structural/magnetic lineation, and perpendicular to the

structural/magnetic foliation, plagioclase and quartz phenocrysts are commonly sheared. Quartz exhibits wavy extinction, and dynamic recrystallized sub-grains elongated parallel to the lineation (Fig. 10E). Pressure shadows developed on the ends of quartz grains, together with the stretched mica bands, define the microscopic foliation (Fig. 10F). Plagioclase grains are characterized by wavy extinction, and cracks (Fig. 10G). Asymmetric quartz pressure shadows formed at the ends of plagioclase (Fig. 10H). A domino structure (Fig. 10I) develops in some plagioclase. Mica fringes developed as curved tails at the tip of quartz clasts (Fig. 10J) The sericite-rich foliation is also deformed by shear bands (Fig. 10K). All the phenomenon listed above indicate a solid-state deformation (Passchier and Trouw, 2005; Vernon, 2000). In the case of low angle structural/magnetic foliation, these shear criteria indicate a top-to-the-NW movement while in the case of highly inclined structural/magnetic foliation, the sense of shear indicates that the NW-side is moving down and SE-side is moving up (Passchier and Trouw, 2005). In the XZ thin-sections parallel to the NE-SW low-inclined structural/magnetic lineation and perpendicular to the structural/magnetic foliation, cracked plagioclase, wavy extinction and elongated quartz sub-grains argue for NE-SW stretching, however, no shear sense was identified.

In thin-sections, rocks sampled at the margins of the syn-tectonic granitoids plutons are characterized by a preferred orientation of plagioclase and K-feldspar. Moreover, the plagioclase grains are bent and quartz-filled fractures are well developed (Fig. 10L and 10M). Quartz grains developed wavy extinction, chessboard

structure and sub-grains. All of these features indicate that these plutons acquired a mineral preferred orientation during their crystallization (Bouchez et al., 1992; Bouchez and Gleizes, 1995; Vernon, 2000), in other word, the crystallization of these granitoids was coeval with a tectonic event (Tribe and Dlemos, 1996).

The isotropic granitoids consist of automorphic K-feldspar, plagioclase, and mica. Neither crystal-plastic deformation nor pervasive mineral preferred orientation has been developed in these rocks. Therefore, the isotropic granite exhibits a typical magmatic texture (Fig. 10 N).

6. Discussion

6.1 Summary of observation and measurement

The magnetic carriers of the samples from the Gneiss Unit, pervasively sub-solidus deformed granitoids, and migmatite, the magmatically deformed syn-tectonic granitoids and the undeformed isotropic granitoids are mainly magnetite while the magnetic carriers for the deformed volcanic rocks are mainly paramagnetic minerals. Thus a conclusion that all the magnetic fabrics acquired in the CNB are normal magnetic ones can be reached. The magnetic anisotropy tensor represents the strain ellipsoid, and thus can be directly used for structural interpretation alike the mineral fabrics observed both in the field and thin section.

In map view, the Gneiss Unit and the Deformed Volcanic Rocks Unit of the CNB strike along the NE-SW direction. Both of the structural/magnetic foliations of these two units also strike along the NE-SW direction, parallel to the cartographic

arrangement of these two units. The variation of dip angles of the structural/magnetic foliation indicates a late folding of the foliation of these two units, which is also supported by the upright and NW verging folds observed in the field.

The structural/magnetic lineation is relatively scattered, as it may be whether parallel to the foliation strike or not. When the lineation trends perpendicular or at high angle to the strike of the foliation, a non-coaxial strain regime with top-to-the-NW sense of shear is commonly observed. In contrast, when the lineation strikes NE-SW with a shallow inclination, kinematic indicators are absent, and a coaxial strain regime is inferred.

The syn-tectonic granitoids of the CNB are usually spindle shaped plutons with a NE-SW long axis. A NE-SW striking magmatic foliation usually developed along the margins of these plutons. The mafic microgranitoid enclaves included in these plutons are oblate and parallel to the magmatic foliation. The textural observations document that the crystallization of the granitic magma was coeval with a regional tectonic event.

In the isotropic granitoids, field observations reveal that the minerals are neither deformed nor oriented. Microscopic observation shows that these rocks have a magmatic texture characterized by automorphic amphibole, K-feldspar, plagioclase, micas and xenomorphic quartz.

Our microstructural analysis shows that along the NE-SW lineation, kinematic indicators are absent, either in the field or in the thin sections, though a minor amount of stretching does exist, as indicated by elongated and recrystallized quartz grains (see

section 5). A coaxial strain regime can be determined along the NE-SW lineation that is therefore interpreted as a B-type structure, i.e. perpendicular to the transport direction, formed during the folding. The NE-SW direction does not represent a regional shearing direction. Thus we argue that this NE-SW shallow inclined B-type lineation was formed during the E_{1b} event. By contrast, the lineation with an original NW-SE direction, and top-to-the-NW shear sense is A-type lineation, which was formed during the E_{1a} event, and represents the displacement direction.

6.2 The relationship between the Gneiss Unit and the Deformed Volcanic Rocks Unit

Since a long time, the relationship between the Gneiss Unit and the Deformed Volcanic Rocks Unit of the CNB is a disputed topic among the geologists. It was first considered that this boundary was an ophiolitic suture (Hsu et al., 1990; Lu et al., 1994; Wang and Lu, 1997). However, typical ophiolitic rocks such as serpentinized peridotite, gabbro, mafic dyke, pillow basalt and siliceous deep-sea sediment are absent there. The scattered gabbro masses that crop out in the Changle-Nan'ao belt are not deformed, and their geochemical characteristics do not match with ophiolitic mafic rocks, but rather with intraplate ones (Zou, 1995; Xu et al., 1999). Other researchers considered that the Deformed Volcanic Rocks Unit unconformably overlaid the Gneiss Unit (Zhu et al, 1993). But the unconformity hypothesis does not account for the structural accordance between the two units in spite of their difference in metamorphic grade, amphibolite and lower green schist facies for the Gneiss Unit and the Deformed Volcanic Rocks Unit, respectively. The Al^{total} in-amphibole geobarometer (Tong and Tobisch 1996) indicates that the syn-tectonic granite

intruding into the Gneiss Unit emplaced at 16 km depth. As these syn-tectonic granites were exposed close to the surface in Late Cretaceous, an exhumation process of the Gneiss Unit must be considered. After calculating the cooling rate provided by the ^{40}Ar-^{39}Ar data, Chen et al. (2002) assumed that thrusting might have played a major role in the exhumation of the Gneiss Unit. However, this hypothesis needed a structural confirmation.

The important difference in metamorphic grade between the Gneiss and the Deformed Volcanic Rocks Unit, was attributed to two different events, namely, the formation of the basement of the Min-Tai microcontinent recorded by the gneissic rocks, and the collision between the Min-Zhe volcanic arc and the Min-Tai microcontinent recorded by the deformed volcanic rocks (Wang and Lu, 1997). However, a single tectonic event can leave different footprints at different crustal depths. The gneissic rocks may just represent a deeper and hotter deformation level compared to the shallow crustal one in the deformed volcanic rocks. The structural consistency, i.e. the NW-SE lineation, and the top-to-the-NW shear sense recorded both units, supports this argument. The fact that the deformation of the Gneiss Unit was more pervasive than that in the Deformed Volcanic Rocks Unit indicates a SE-ward increase in deformation intensity.

In this study, the boundary between the Gneiss Unit and the Deformed Volcanic Rocks Unit was observed in the Fuqing area. On both sides of the boundary, the shear senses indicate that the NW-side is moving down and SE-side moving up (Figs. 2G and 2H). This geometry has two possible interpretations: 1) these two units contact

with each other by a normal fault along which the Deformed Volcanic rocks Unit is the hanging wall and the Gneiss Unit the footwall; or 2) these two units contact with each other by a thrust fault in which the Deformed Volcanic rocks Unit is the footwall and the Gneiss Unit is the hanging wall. Considering the general evolution of the CNB during the Cretaceous, if the contact was a normal fault, it should have been active during the E_2 event. However, tension gash opening, and plutons and dyke emplacement without developing normal faulting characterize the E_2 event. Thus, we prefer to interpret the contact between the Gneiss Unit and the Deformed Volcanic Rocks unit as a thrust fault. Nevertheless a ductile normal fault cannot be ruled out. Further studies are needed to settle this point.

6.3. Deformation age of the E_1 event of Changle-Nan'ao belt

Owing to the widespread Late Cretaceous magmatism, the ^{40}Ar-^{39}Ar chronometer may have been reset and does not always indicate the age of the E_1 event (Li et al., 2003; Li et al., 2014). Recent zircon U-Pb dating of granite and volcanic rocks in the study area show that the youngest age of the deformed volcanic rocks involved in E_1 is 130 Ma, and the oldest age of the undeformed volcanic rocks is 104 Ma (Guo et al., 2012). The Late K_1 period is also the time of emplacement of the Duxun (120 Ma), Weitou (108 Ma), Geshan (131 Ma), Sucuo (130 Ma) and Niutouwei (130 Ma) syntectonic granitoids (Li et al., 2003; Liu et al., 2012; Cui et al., 2013; locations 4, 5, 6, 9 in Fig. 3). Thus a ca. 130-105 Ma age is reasonably proposed for the E_1 event.

6.4 Polyphase tectonics in the CNB

In this section, a possible crustal scale tectonic evolution scenario of the CNB during the Cretaceous is proposed (Fig. 11). Based on field observations and laboratory analyses, we divided the Late Mesozoic tectonics of CNB into E_1, E_2 and E_3 tectonic and magmatic events (cf. section 3). Moreover, we must also consider an earlier E_0 event of Early Cretaceous (Berriasian-Valanginian, 140-130 Ma) age, during which numerous plutons and volcanic rocks with magmatic arc affinity emplaced (Fig. 11A). The deformation features associated with the E_0 event are not recognized yet, partly due to the pervasive deformation developed during the E_1 event. Presently, only a magmatic activity can be confidently attributed to the E_0 event.

During the Early Cretaceous, around Barremian-Albian (130-105 Ma), the granitic plutons and their host-rocks experienced a ductile shearing coeval with an amphibolite facies metamorphism. These rocks were thrust to the NW upon sedimentary and volcanic rocks in which ductile shear zones developed. Also during this period, a new generation of granitoids, dominantly two-mica peraluminous and migmatite, formed at the expense of continental crust (Figs. 3, and 11B).

At the end of the Early Cretaceous, in Albian, upright or NW-SE verging folds accommodated the NW-SE shortening (Fig. 11C). On the rims of the Early Cretaceous syntectonic plutons, the NE-SW striking highly inclined magmatic foliation also argues for a NW-SE shortening (Figs. 3 and 5A).

At the beginning of the Late Cretaceous, from Albian to Turonian (105-90 Ma) the E_2 event is represented by the opening of NE-SW striking brittle cracks filled by granitic magma (Fig. 11D). These dykes are recognized all along the South China

coastal area (Zhou et al., 2006; Dong et al., 2010; Chen et al., 2014). This suggests that the area experienced an extensional event. The numerous A-type plutons emplaced in the Late Cretaceous also argue for such a tectonic setting (Li et al., 2014). Moreover, the statistical measurement of the brittle cracks that cross cut previously deformed, or undeformed rocks, indicates a NW-SE stretching direction (Xu et al., 2014). However, extension-related mid-scale structures and ductile deformations such as graben or half-graben basins, detatchment faults or MCC are not documented in the study area.

Since a long time, the CNB has been regarded as a ductile strike-slip fault due to the observation of a NE-SW lineation which is parallel to the foliation strike mainly in Dongshan island, or a lineation which is oblique to the strike of foliation mainly in the rest of CNB, and the discovery of cm-wide mylonitic shear zones (Charvet et al., 1990; Tong and Tobisch, 1996; Wang and Lu, 2000). Our field and AMS studies acknowledge the previous observations, however our interpretation differs as follows. 1) The weakly inclined foliation with a NW-SE lineation in numerous sites does not support the existence of a NE-SW strike-slip fault (e.g. locations 3 and 5 in Fig. 3). 2) When the foliation is subvertical, or at a high-angle, we argue that the present geometry results of a late folding, but the foliation was formed with a sub-horizontal, or low angle attitude. After restoring S_1 to horizontal, the oblique lineation strikes NW-SE, and the shear sense is consistently top-to-the-NW (Figs. 3, 5E and 5F). 3) Regardless of the origin of the NE-SW horizontal stretching lineation, its rare abundance, local occurrence, mainly in Dongshan island, and the absence of shear

sense reduce the possibility of a significant strike-slip faulting. 4) The E_3 mylonitic shear zones belonging to a late event do not correspond to a major strike-slip fault.

6.5 Geodynamic setting of the Changle-Nan'ao Belt

In the Late Mesozoic, the East Asia Continental Margin experienced several tectonic events related to the Paleo-Pacific-Eurasia convergence. The SW Japan nappes, the Tananao metamorphic complex in Taiwan, and the ophiolite nappe and olistostrome complex in the West Philippines argue for the subduction and closure of a Paleo-Pacific oceanic basin (Faure et al., 1986; Faure, 1987; Faure, M., Natalin, B., 1992; Wakita and Metcalfe, 2005; Yui et al., 2012; Hall, 2012; Wakita, 2013; Saito et al., 2014).

When discussing the Mesozoic geodynamic significance of the CNB, it is necessary to consider the surrounding areas, and particularly the West Philippines islands. The Philippines archipelago is divided into the Philippine Mobile Belt, represented by the east Philippines islands, and the West Philippine Domain. The former consists of several ophiolitic series and subduction complexes with an oceanic plate stratigraphy, which experienced an evolution history including accretion and collision since the Cretaceous, as this domain is beyond the scope of this study, it will not be discussed in the following. The latter is frequently referred to as a microcontinent that collided with the Philippine Mobile Belt in the Cenozoic (e.g. Yumul et al., 2003, 2009). However, given that the existence of a Mesozoic ophiolitic suite in the Palawan or Mindoro islands, the West Philippines Domain itself results of a complex evolution (Casasola, 1956).

Several lines of evidence support the previous interpretation that the West Philippine Domain was once located immediately South of the SCB in the late Mesozoic time (Holloway, 1982; Faure et al., 1989; Faure and Natal'in, 1992; Almasco et al., 2000). Firstly, paleomagnetic studies indicate that the West Philippines islands, such as Mindoro and North Palawan, were once at the same latitude as the eastern margin of South China (Almasco et al., 2000 and references therein), secondly, the Late Cretaceous rhyolite cropping out in Mindoro has been correlated with a contemporary rhyolite exposed in the CNB (Knittel 2011), thirdly, detrital zircon in North Palawan sandstone shows a northern provenance from Mesozoic rocks of the SCB margin (Suggate et al, 2014)..Thus the West Philippines Domain appears as a composite terrane resulting of continental collision between SCB and a west Philippines microcontinent. In Palawan and nearby islands, the Mid-Late Jurassic olistostrome and south-directed ophiolite nappe upon a continental crust have been interpreted as the products of a North-directed subduction, and subsequent collision of the West Philippines microcontinent with the SCB (Faure et al., 1989; Faure and Natal'in, 1992). The precise age of the collision is not well settled, however it certainly took place after the stratigraphic age of the ophiolite suite and before the Lutetian (ca 42 Ma) during which a granite intruded into the stack of nappes (Suggate et al, 2014). Since the Eocene, the East Asia Continental Margin experienced an important rifting event during which a number of marginal sea basins opened. Consequently, the West Philippines Domain including a piece of the SCB lithosphere and the West Philippine microcontinent was separated from South China continent

(Briais et al., 1993; Yin, 2010; Barckhausen et al., 2014). In this process, the opening of South China Sea led to the clockwise rotation of the West Philippine Domain represented by North Palawan and the smaller nearby islands (Zhou et al., 1995; Almasco et al., 2000). The available geological data of the Western Philippines comply with the interpretation that during the Early to Middle Cretaceous, an ophiolitic suture, and SE-directed nappes developed SE of the CNB. Considering the tectonic relationships and the contemporaneous activity between the CNB and West Philippines Domain, the late Early Cretaceous, between 130-105 Ma, might be a possible age for the collision of the West Philippine microcontinent with SCB. In the CNB, the E_1 event with a top-to-the-NW sense of shear could be viewed as a back-thrusting tectonic event with respect to the West Philippines microcontinent collision with the South China block (Fig. 12).

The tectonics recorded by the E_1 thrust event of the CNB is an example of the complexity of the convergence pattern between East Asia and Paleo-Pacific that cannot be only depicted as a simple active continental margin. Though, at least since the Jurassic, the oceanic subduction of the Paleo-Pacific plate was responsible for the formation of a magmatic arc, many “terranes” such as microcontinents, oceanic islands and other buoyant features accreted along the East Asia Continental Margin (Faure and Natalin, 1992; Sengor and Natalin, 1996; Hara and Kurihara, 2010; Wakita, 2013; Safonova and Santosh, 2014). The collision of such microcontinents with Eurasia produced a widely distributed deformation on the continental margin.

After the E_1 event, the E_2 one, is represented by emplacement of dyke and

granitoid, including A-type plutons throughout the study area (Li et al., 2014). Considering that the emplacement of the granitoids during E_2 event did not alter the fabrics of the country rocks near the pluton boundary, the emplacement mechanism may well be a passive one in which the room occupied was created by regional extension (e.g. Wei et al., 2014b). Together with the NE-SW striking dykes in the southeast coast area (Dong et al., 2006; Zhou et al., 2006; Dong et al., 2010; Chen et al., 2014), this suggests that after the completion of the shortening E_1 event in the South China Block, which was caused by the collision between the South China Block and the West Philippine Microcontinent, was followed by a post-collisional extensional regime in the South China coastal area.

Though structural data to support the change from the compressive to extensive tectonic regime remain to be further documented, the newly acquired petrological and geochemical data provide a good vision of this shift. During the E_1 event, the magmatic rocks are mainly high K calc-alcaline to shoshonitic rhyolite, dacite, and I-type granitoids (Guo et al., 2012; Liu et al., 2012). The volcanic rocks of this age are characterized by enriched LILE, LREE, depleted Nb and Ta, high initial $^{87}Sr/^{86}Sr$, negative εNd(T) while the coeval plutonic rocks are characterized by enriched LILE, LREE, depleted HFSE, high initial $^{87}Sr/^{86}Sr$, negative εNd(T), and negative εHf(T) indicating that these kind of igneous rocks were originated from arc-related enriched mantle (Lapierre et al., 1997; He and Xu, 2012; Liu et al., 2012). By contrast, during the E_2 event, the magmatic rocks are featured by the appearance of bimodal volcanic series and A-type granitoids with miarolitic structure (Qiu et al., 1999; Zhou et al.,

2006). The geochemical features of the igneous rocks of the E_2 event are similar to the older igneous, however their εNd(T) and εHf(T) values are higher than those of the E_1 rocks, which indicate an asthenospheric influence (He and Xu, 2012). This geochemical difference has been interpreted as an indication of a shift from compression to extension caused by the retreat of the subducting slab, and upwelling of asthenosphere (He and Xu, 2012).

7. Conclusions

Combined with the available geochronological data, our detail structural analysis and AMS investigation of the CNB allows us to reappraise the tectonic scenario of the SE coast of the SCB. Our model, at variance with previous ones, proposes that during the late Early Cretaceous (Barremian to Albian), between 130 and 105 Ma, a NW-directed ductile thrust, represented by a NE-SW striking low-angle foliation, and NW-SE directed stretching lineation with a top-to-the-NW sense of shear developed during the E_{1a} event. The NE-SW folding of the foliation during E_{1b} was still a consequence of the same NW-SE shortening. Syn-tectonic plutons also emplaced during the E_1 phase. This NW-directed thrust is considered as a back-thrust toward the Asia continent developed in response of the collision of the West Philippines microcontinent with the South China block. During the 104-90 Ma period, bimodal and alkaline lava flows, post-collision granitoids and dykes emplaced probably in an extensional setting (E_2). Our results suggest that the Late Mesozoic tectonics of the East Asia Continental Margin were controlled by microcontinent collision and

subsequent extension rather than by continental scale strike-slip faulting.

Acknowledgments

This study was funded by NSFC (41225009), Grant No. 2011ZX05008-001, the grant of Ministry of Land and Resources (201211024-04) and China Postdoctoral Science Foundation (Grant No. 2014M561036)

.

References

Almasco, J., Rodolfo, K., Fuller, M., Frost, G., 2000. Paleomagnetism of Palawan, Philippines. Journal of Asian Earth Sciences 18, 369-389.

Barckhausen, U., Engels, M., Franke, D., Ladage, S., and Pubellier, M., 2014, Evolution of the South China Sea: Revised ages for breakup and seafloor spreading: Marine and Petroleum Geology 58, 599-611.

Blumenfeld, P., and Bouchez, J.-L., 1988. Shear criteria in granite and migmatite deformed in the magmatic and solid states. Journal of Structural Geology 10, 361-372.

Borradaile, G.J. and Henry, B., 1997. Tectonic applications of magnetic susceptibility and its anisotropy. Earth-Science Reviews 42, 49-93.

Bouchez, J.L., Delas, C., Gleizes, G., Nedelec, A., Cuney, M., 1992. Submagmatic microstructure in granites. Geology 20, 35-38.

Bouchez, J.L. and Gleizes, G., 1995. Two-stage deformation of the

Mont-Louis-Andorra granite pluton (Variscan Pyrenees) inferred from magnetic-susceptibility anisotropy. Journal of the Geological Society 152, 669-679.

Briais, A., Patriat, P., Tapponnier, P. 1993. Updated interpretation of magnetic anomalies and sea floor spreading stages in the South China Sea: Implications for the Tertiary Tectonics of Southeast Asia. J. Geophys. Reasearch 98, 6299-6328.

Casasola, A.G., 1956. Geological reconnaissance of southern Palawan. The Philippine Geologist 10, 76-88.

Charvet, J., Faure, M., Xu, J.W., Zhu, G., Tong, W.X., Lin, S.F., 1990. The Changle-Nanao tectonic zone, south east china. Comptes Rendus de l'Académie des Sciences Série II 310, 1271-1278.

Chen, N.-H., Dong, J.-J., Chen, J.-Y., Dong, C.-W., Shen, Z.-Y., 2014. Geometry and emplacement of the Late Cretaceous mafic dyke swarms on the islands in Zhejiang Province, Southeast China: Insights from high-resolution satellite images. Journal of Asian Earth Sciences 79, Part A, 302-311.

Chen, W.S., Yang, H.C., Wang, X., Huang, H., 2002. Tectonic setting and exhumation history of the Pingtan-Dongshan Metamorphic Belt along the coastal area, Fujian Province, Southeast China. Journal of Asian Earth Sciences 20, 829-840.

Cui, J.J., Zhang, Y.Q., Dong, S.W., Jahn, B.M., Xu, X.B., Ma, L.C., 2013. Zircon U-Pb geochronology of the Mesozoic metamorphic rocks and granitoids in the coastal tectonic zone of SE China: Constraints on the timing of Late Mesozoic

orogeny. Journal of Asian Earth Sciences 62, 237-252.

Dong, C.W., Yan, Q., Zhang, D.R., Du, Z.Y., Zhu, G.Q., 2010. Late Mesozoic extension in the coastal area of Zhejiang and Fujian provinces: A petrologic indicator from the Dongji Island mafic dike swarms. Acta Petrologica Sinica 26, 1195-1203.

Dong, C.W., Zhang, D.R., Xu, X.S., Yan, Q., Zhu, G.Q., 2006. SHRIMP U-Pb Dating and lithogeochemistry of basic-intermediate dike swarms from Jinjiang, Fujian Province. Acta Petrologica Sinica 22, 1696-1702.

Dunlop, D.J., 2002. Theory and application of the Day plot (M-rs/M-s versus H-cr/H-c) 1. Theoretical curves and tests using titanomagnetite data. Journal of Geophysical Research-Solid Earth 107.

Faure, M., 1987. Spéculations sur l'accrétion de l'Asie au Mésozoïque par collisions et coulissement de microblocs. Comptes Rendus de l'Académie des Sciences Série II 304, 93-98.

Faure, M., Caridroit, M., Charvet, J., 1986. The late Jurassic oblique collisional orogen of SW Japan. New structural data and synthesis. Tectonics 5, 1089-1114.

Faure, M., Caridroit, M., Guidi, A., Charvet, J., 1987. The Late Jurassic orogen of south west Japan: nappe tectonics and longitudinal displacement. Bulletin de la Société Géologique de France 3, 477-485.

Faure, M., Lin, W., Scharer, U., Shu, L.S., Sun, Y., Arnaud, N., 2003. Continental subduction and exhumation of UHP rocks. Structural and geochronological insights from the Dabieshan (East China). Lithos 70, 213-241.

Faure, M., Marchadier, Y., Rangin, C., 1989. Pre-eocene synmetamorphic structure in the Mindoro-Romblon-Palawan area, west philippines, and mplications for the history of southeast asia. Tectonics 8, 963-979.

Faure, M. and Natalin, B., 1992. The geodynamic evolution of the eastern Eurasian margin in Mesozoic times. Tectonophysics 208, 397-411.

Ferre, E.C., Gebelin, A., Till, J.L., Sassier, C., and Burmeister, K.C., 2014, Deformation and magnetic fabrics in ductile shear zones: A review: Tectonophysics 629, 179-188.

Gilder, S.A., Gill, J., Coe, R.S., Zhao, X.X., Liu, Z.W., Wang, G.X., Yuan, K.R., Liu, W.L., Kuang, G.D., Wu, H.R., 1996. Isotopic and paleomagnetic constraints on the Mesozoic tectonic evolution of south China. Journal of Geophysical Research - Solid Earth 101, 16137-16154.

Guo, F., Fan, W.M., Li, C.W., Zhao, L., Li, H.X., Yang, J.H., 2012. Multi-stage crust-mantle interaction in SE China: Temporal, thermal and compositional constraints from the Mesozoic felsic volcanic rocks in eastern Guangdong-Fujian provinces. Lithos 150, 62-84.

Hall, R., 2012. Late Jurassic–Cenozoic reconstructions of the Indonesian region and the Indian Ocean. Tectonophysics 570, 1-41.

Hara, H. and Kurihara, T., 2010. Tectonic evolution of low-grade metamorphosed rocks of the Cretaceous Shimanto accretionary complex, Central Japan. Tectonophysics 485, 52-61.

He, T. and Zhang, X., 1989. Phanerozoic metamorphism and crustal evolution in the

southeastern part of China. Journal of Southeast Asian Earth Sciences 3, 321-330.

He, Z.Y. and Xu, X.S., 2012. Petrogenesis of the Late Yanshanian mantle-derived intrusions in southeastern China: Response to the geodynamics of paleo-Pacific plate subduction. Chemical Geology 328, 208-221.

Holloway, N., 1982. North Palawan Block, Philippines; its relation to Asian mainland and role in evolution of South China Sea. AAPG Bulletin 66, 1355-1383.

Hsu, K.J., Li, J.L., Chen, H.H., Wang, Q.C., Sun, S., Sengor, A.M.C., 1990. Tectonics of South China: key to understanding west Pacific geology. Tectonophysics 183, 9-39.

Jahn, B.M., 1974. Mesozoic Thermal Events in Southeast China. Nature 248, 480-483.

Jelinek, V., 1981. Characterization of the magnetic fabric of rocks. Tectonophysics 79, T63-T67.

Knittel, U., 2011, 83 Ma rhyolite from Mindoro - evidence for Late Yanshanian magmatism in the Palawan Continental Terrane (Philippines). Island Arc 20, 138-146.

Lapierre, H., Jahn, B.M., Charvet, J., Yu, Y.W., 1997. Mesozoic felsic arc magmatism and continental olivine tholeiites in Zhejiang province and their relationship with the tectonic activity in southeastern China. Tectonophysics 274, 321-338.

Li, J.H., Zhang, Y.Q., Dong, S.W., Su, J.b., Li, Y., Cui, J.J., Shi, W., 2013. The Hengshan low-angle normal fault zone: structural and geochronological

constraints on the Late Mesozoic crustal extension in South China. Tectonophysics 606, 97-115.

Li, W.X., Zhou, X.M., Li, X.H., 2003. U-Pb and $^{40}Ar/^{39}Ar$ dating of deformed igneous rocks from the Changle-Nan'ao fault. Chinese Journal of Geology 38, 22-30.

Li, X.H., 2000. Cretaceous magmatism and lithospheric extension in Southeast China. Journal of Asian Earth Sciences 18, 293-305.

Li, Z., Qiu, J.S., Yang, X.M., 2014. A review of the geochronology and geochemistry of Late Yanshanian (Cretaceous) plutons along the Fujian coastal area of southeastern China: Implications for magma evolution related to slab break-off and rollback in the Cretaceous. Earth-Science Reviews 128, 232-248.

Li, Z.X. and Li, X.H., 2007. Formation of the 1300-km-wide intracontinental orogen and postorogenic magmatic province in Mesozoic South China: A flat-slab subduction model. Geology 35, 179-182.

Li, Z.X., Li, X.H., Chung, S.L., Lo, C.H., Xu, X.S., Li, W.X., 2012. Magmatic switch-on and switch-off along the South China continental margin since the Permian: Transition from an Andean-type to a Western Pacific-type plate boundary. Tectonophysics 532, 271-290.

Liu, Q., Yu, J.H., Wang, Q., Su, B., Zhou, M.F., Xu, H., Cui, X., 2012. Ages and geochemistry of granites in the Pingtan-Dongshan Metamorphic Belt, Coastal South China: New constraints on Late Mesozoic magmatic evolution. Lithos 150, 268-286.

Lu, H., Jia, D., Wang, Z., Guo, L., Shi, Y., Zhang, Q., 1994. Tectonic evolution of the Dongshan terrane, Fujian province, China. Journal of South American Earth Sciences 7, 349-365.

Passchier, C.W., Trouw, R.A., 2005. Microtectonics. Springer, Berlin.

Paterson, S.R., Vernon, R.H., Tobisch, O.T., 1989. Areview of criteria for the identification of magmatic and tectonic foliations in granitoids. Journal of Structural Geology 11, 349-363.

Qiu, J.S., Wang, D.Z., and Zhou, J.C., 1999, Geochemistry and petrogenesis of the Late Mesozoic Bimodal volcanic rocks at Yunshan Caldera, Yongtai County, Fujian Province: Acta Petrologica et Mineralogica 18, 97-107.

Safonova, I.Y. and Santosh, M., 2014. Accretionary complexes in the Asia-Pacific region: tracing archives of ocean plate stratigraphy and tracking mantle plumes. Gondwana Research 25, 126-158.

Saito, T., Okada, Y., Fujisaki, W., Sawaki, Y., Sakata, S., Dohm, J., Maruyama, S., Hirata, T., 2014. Accreted Kula plate fragment at 94Ma in the Yokonami-melange, Shimanto-belt, Shikoku, Japan. Tectonophysics 623, 136-146.

Sengör, A.C. and Natal'in, B.A., 1996. Turkic-type orogeny and its role in the making of the continental crust. Annual Review of Earth and Planetary Sciences 24, 263-337.

Shu, L.S., Zhou, X.M., Deng, P., Wang, B., Jiang, S.Y., Yu, J.H., Zhao, X.X., 2009. Mesozoic tectonic evolution of the Southeast China Block: New insights from

basin analysis. Journal of Asian Earth Sciences 34, 376-391.

Suggate, S.M., Cottam, M.A., Hall, R., Sevastjanova, I., Forster, M.A., White, L.T., Armstrong, R.A., Carter, A., Mojares, E., 2014. South China continental margin signature for sandstones and granites from Palawan, Philippines. Gondwana Research 26, 699-718.

Talbot, J-Y., Martelet, G., Courrioux, G., Chen Y., Faure, M., 2004. Emplacement in an extensional setting of the Mont Lozère-Borne granitic complex (SE France) inferred from comprehensive AMS, structural and gravity studies. J. Struct. Geol., 26, 11-28.

Tarling, D.H. and Hrouda, F., 1993. The magnetic anisotropy of rocks. Chapman & Hall, London.

Tong, W.X. and Tobisch, O.T., 1996. Deformation of granitoid plutons in the Dongshan area, southeast China: Constraints on the physical conditions and timing of movement along the Changle-Nanao shear zone. Tectonophysics 267, 303-316.

Tribe, I.R. and D'lemos, R.S., 1996. Significance of a hiatus in down-temperature fabric development within syntectonic quartz diorite complexes, Channel Islands, UK. Journal of the Geological Society 153, 127-138.

Van der Molen, I. and Paterson, M., 1979, Experimental deformation of partially melted granite. Contributions to Mineralogy and Petrology 70, 299-318.

Vernon, R., 1986, K-feldspar megacrysts in granites - phenocrysts, not porphyroblasts. Earth-Science Reviews 23, 1-63.

Vernon, R., Paterson, S., and Geary, E., 1989, Evidence for syntectonic intrusion of plutons in the Bear Mountains fault zone, California. Geology 17, 723-726.

Vernon, R., 2000. Review of microstructural evidence of magmatic and solid-state flow. Visual Geosciences 5, 1-23.

Wakita, K., 2013. Geology and tectonics of Japanese islands: A review–The key to understanding the geology of Asia. Journal of Asian Earth Sciences 72, 75-87.

Wakita, K. and Metcalfe, I., 2005. Ocean plate stratigraphy in East and Southeast Asia. Journal of Asian Earth Sciences 24, 679-702.

Wang, D. and Shu, L., 2012. Late Mesozoic basin and range tectonics and related magmatism in Southeast China. Geoscience Frontiers 3, 109-124.

Wang, Y., Fan, W., Zhang, G., Zhang, Y., 2013. Phanerozoic tectonics of the South China Block: key observations and controversies. Gondwana Research 23, 1273-1305.

Wang, Z.H. and Lu, H.F., 1997. Evidence and dynamics for the change of strike-slip direction of the Changle-Nanao ductile shear zone, southeastern China. Journal of Asian Earth Sciences 15, 507-515.

Wang, Z.H. and Lu, H.F., 2000. Ductile deformation and $^{40}Ar/^{39}Ar$ dating of the Changle-Nanao ductile shear zone, southeastern China. Journal of Structural Geology 22, 561-570.

Wei, W., Chen, Y., Faure, M., Shi, Y.H., Martelet, G., Hou, Q.L., Lin, W., Le Breton, N., Wang, Q.C., 2014a. A multidisciplinary study on the emplacement mechanism of the Qingyang–Jiuhua Massif in Southeast China and its tectonic

bearings. Part I: Structural geology, AMS and paleomagnetism. Journal of Asian Earth Sciences 86, 76-93.

Wei, W., Martelet, G., Le Breton, N., Shi, Y., Faure, M., Chen, Y., Hou, Q., Lin, W., Wang, Q., 2014b. A multidisciplinary study of the emplacement mechanism of the Qingyang–Jiuhua massif in Southeast China and its tectonic bearings. Part II: Amphibole geobarometry and gravity modeling. Journal of Asian Earth Sciences 86, 94-105.

Xu, J., Zhu, G., Tong, W., Cui, K., Liu, Q., 1987. Formation and evolution of the Tancheng-Lujiang wrench fault system: a major shear system to the northwest of the Pacific Ocean. Tectonophysics 134, 273-310.

Xu, X., Dong, C., Li, W., Zhou, X., 1999. Late Mesozoic intrusive complexes in the coastal area of Fujian, SE China: the significance of the gabbro-diorite–granite association. Lithos 46, 299-315.

Xu, X.B., Li, Y., Xue, D.J., Xie, M.Y., Tang, S., Cui, J.J., and Zhang, Y.Q., 2014, Deformation characteristics and geochronological constraints of Late Mesozoic extensional structure in Quanzhou, Fujian Province: Earth Science Journal of China University of Geoscience, v. 39, p. 45-63.

Yang, Y.-T., 2013. An unrecognized major collision of the Okhotomorsk Block with East Asia during the Late Cretaceous, constraints on the plate reorganization of the Northwest Pacific. Earth-Science Reviews 126, 96-115.

Yin, A., 2010. Cenozoic tectonic evolution of Asia: A preliminary synthesis. Tectonophysics 488, 293-325.

Yui, T.F., Maki, K., Lan, C.Y., Hirata, T., Chu, H.T., Kon, Y., Yokoyama, T.D., Jahn, B.M., and Ernst, W.G., 2012, Detrital zircons from the Tananao metamorphic complex of Taiwan: Implications for sediment provenance and Mesozoic tectonics: Tectonophysics 541, 31-42.

Yumul, G.P., Dimalanta, C.B., Tamayo, R.A., and Maury, R.C., 2003, Collision, subduction and accretion events in the Philippines: A synthesis. Island Arc 2, 77-91.

Yumul Jr, G.P., Dimalanta, C.B., Marquez, E.J., and Queaño, K.L., 2009, Onland signatures of the Palawan microcontinental block and Philippine mobile belt collision and crustal growth process: A review. Journal of Asian Earth Sciences 34, 610-623.

Zhou, D., Ru, K., Chen, H.-z., 1995. Kinematics of Cenozoic extension on the South China Sea continental margin and its implications for the tectonic evolution of the region. Tectonophysics 251, 161-177.

Zhou, X.M. and Li, W.X., 2000. Origin of Late Mesozoic igneous rocks in Southeastern China: implications for lithosphere subduction and underplating of mafic magmas. Tectonophysics 326, 269-287.

Zhou, X.M., Sun, T., Shen, W.Z., Shu, L.S., Niu, Y.L., 2006. Petrogenesis of Mesozoic granitoids and volcanic rocks in South China: A response to tectonic evolution. Episodes 29, 26-33.

Zhu, G., Jiang, D., Zhang, B., Chen, Y., 2012. Destruction of the eastern North China Craton in a backarc setting: Evidence from crustal deformation kinematics.

Gondwana Research 22, 86-103.

Zhu, G., Niu, M.L., Xie, C.L., Wang, Y.S., 2010. Sinistral to Normal Faulting along the Tan-Lu Fault Zone: Evidence for Geodynamic Switching of the East China Continental Margin. Journal of Geology 118, 277-293.

Zhu, G., Xu, J.W., Gao, D.L., Lin, S.F., Ma, G.F., 1993. structural characteristics and deformation of the Changle-Nan'ao mega shear zone along the southeast China coast, In: Xu, J.W., The Tancheng-Lujiang Wrench Fault System. Wiley, Chichester, pp. 201-209.

Zou, H.B., 1995. A mafic-ultramafic rock belt in the Fujian coastal area, southeastern China: A geochemical study. Journal of Southeast Asian Earth Sciences 12, 121-127.

Figure and table captions

Figure 1. A: Sketch map of the present East Asia Continental Margin geodynamics. NCB: North China Block; TLF: Tan-Lu fault; QDO: Qinling-Dabie Orogen; SCB: South China Block; CNB: Changle-Nan’ao Belt; SCS: South China Sea; LZ: Luzon Island; PLW: Palawan Island. B: Sketch geologic map of the Changle-Nan’ao Belt.

Figure 2. A: E_1 pervasively deformed granitoid (orthogneiss) in sub-solidus state (GPS: 25.45° N, 119.51° E); B: E_{1b} NW verging fold with NE-SW axis in the Dongshan island (GPS: 23.60° N, 117.43° E); C: E_{1a} mylonitic granitoid, section

parallel to the lineation and perpendicular to the foliation (GPS: 23.74° N, 117.59° E); D: amphibole gneiss with down-dip lineation formed by oriented amphiboles (GPS: 24.63° N, 118.41° E); E: migmatite with folded foliation (GPS: 23.69° N, 117.34° E); F: mylonitic volcanic rocks with asymmetric kinks, section parallel to the lineation and perpendicular to the foliation (GPS: 24.96° N, 118.34° E); G: asymmetric fold of mylonitic volcanic rocks indicating NW-side-moving down and SE-side-moving up sense of shear, near the boundary between the Deformed Volcanic Rocks Unit and the Gneiss Unit (GPS: 25.47° N, 119.44° E); H: shear bands of mylonitic volcanic rocks indicating a NW-side-moving down and SE-side-moving up sense of shear, near the boundary between the Deformed Volcanic Rocks Unit and the Gneiss Unit (GPS: 25.47° N, 119.44° E); I: Early Cretaceous syn-tectonic granitoid with oriented minerals near the boundary of the pluton with country rocks (GPS: 25.58° N, 119.69° E); J: Late Cretaceous granitoid with undeformed minerals (GPS: 24.64° N, 118.58° E); K: E_3 NE-SW striking cm-sized mylonitic shear zone crosscutting Late Cretaceous an undeformed isotropic granitoid (GPS: 25.40° N, 119.52° E); L: Undeformed Late Cretaceous volcanic rocks (GPS: 25.70° N, 119.29° E).

Figure 3. Representative field observed fabric and laboratory measured magnetic fabric of CNB and their structural interpretation. The dip of the foliation/magnetic foliation and the plunge of the lineation/magnetic lineation, please refer to Appendix 2.

Figure 4. NW-SE representative cross sections illustrating the bulk architecture of the Changle-Nan'ao Belt. Profile locations refer to line AA', BB', CC' and DD' in Fig. 1B.

Figure 5. Equal-area lower hemisphere projections of total fabrics of the Changle-Nan'ao Belt. A: foliation pole of gneiss, syn-tectonic granitoid, E_3 shear zone, and strike of E_2 dykes; B: foliation pole of deformed volcanic rocks; C: lineation of E_1 gneiss, E_1 sub-solidus granitoid and E_3 narrow shear zone; D: lineation of deformed volcanic rocks; E: lineation of gneiss, E_1 sub- solidus granitoid and E_3 shear zone after correcting foliation to flat; F: lineation of deformed volcanic rocks after correcting foliation to flat. Solid and open circles/rectangles represent E_1 field and AMS foliation/A-type lineation. Solid and open diamonds represent E_1 field and AMS B-type lineation, Triangle and cross represent sub-solidus field foliation and B-type lineation, reverse triangle represents strike of E_2 dykes, Star and oblique cross represent E_3 foliation and lineation, respectively. The stereo projection of the AMS ellipsoid, please refer to Appendix 3.

Figure 6. Distribution of the bulk magnetic susceptibility of magmatic rocks in the Changle-Nan'ao Belt.

Figure 7. Thermal-Susceptibility, Isothermal Remanent Magnetization (IRM),

Hysteresis Loop diagram of the deformed rocks of the Changle-Nan'ao Belt. The analyzed samples are located in Table 1.

Figure 8. Day-plot diagram of measured samples of the Changle-Nan'ao Belt to define the magnetite size. Mrs: saturation remanence, Ms: saturation magnetization, Hcr: remanent coercive force Hcf: ordinary coercive force, SD: single domain, PSD: pseudo-single domain, MD: multi-domain.

Figure 9. AMS scalar parameters for each site and main lithologies. A: P_J (corrected anisotropy degree) vs. Km (mean bulk magnetic susceptibility in 10^{-3} SI); B: T (shape parameter) vs. P_J (corrected anisotropy degree). The calculations of T and P_J can be found in Jelinek (1981).

Figure 10. Microscopic photo of the rocks in the CNB. A: In the pervasively post-solidus deformed granitoid, quartz grains were stretched and plastically deformed (GPS: 23.74° N, 117.59° E); B: In the pervasively post-solidus deformed granitoid, stretched quartz grains experienced a dynamic recrystallization responsible for the development of an oblique shape fabric indicating a top-to-the-NW shear sense (GPS: 23.75° N, 117.60° E); C: In the pervasively post-solidus deformed granitoid, quartz grains were deformed with a sigmoidal shape indicating a top-to-the-NW shear sense (GPS: 23.76° N, 117.61° E); D: Kinked micas overturned to NW showing a NW-SE shortening (GPS: 23.60° N, 117.43° E); E: In the deformed volcanic rocks,

quartz was dynamic recrystallized, and newly formed tiny quartz neograins elongated parallel to the stretching lineation (marked by the dashed line) (GPS: 25.55° N, 119.35° E); F: In the deformed volcanic rocks, quartz develops pressure shadow, and mica is stretched parallel to the lineation (GPS: 24.96° N, 118.34° E); G: In the deformed volcanic rocks, plagioclase was cracked and boudinaged (GPS: 25.62° N, 119.36° E); H: In the deformed volcanic rocks, asymmetric pressure shadow indicates a top-to-the NW shear sense (GPS: 25.53° N, 119.71° E); I: In the deformed volcanic rocks, the plagioclase is cracked and developed domino structure indicating a top-to-the-NW shear sense (GPS: 25.20° N, 118.58° E); J: In the deformed volcanic rocks, quartz with mica tails indicating a top-to-the-NW shear sense (GPS: 25.59° N, 119.31° E); K: In the deformed volcanic rocks, shear band indicates a top-to-the-NW shear sense (GPS: 25.59° N, 119.31° E); L: At the margin of syn-tectonic granitoid pluton, plagioclase was bent and cracked; the cracks do not penetrate into the granite matrix (GPS: 24.89° N, 118.45° E); M: At the margin of syn-tectonic granitoid pluton, cracked plagioclase infilled with quartz (GPS: 24.91° N, 118.45° E); N: The isotropic granitoids exhibit a magmatic texture with no deformed minerals (GPS: 23.85° N, 117.48° E).

Figure 11. Crustal-scale structural evolution model of the Changle-Nan'ao Belt during the Cretaceous. A: at ca. 140-130 Ma, voluminous magmatism represented by extensive volcanism and plutonism throughout the belt; B: during the E_{1a} event starting at ca. 130 Ma, the belt experienced a top-to-the-NW shearing event

characterized by the development of weakly inclined mylonitic zones in the Deformed Volcanic Rocks Unit, and pervasive post solidus deformation in the Gneiss Unit. In both units, the ductile shearing is represented by a NW-SE stretching lineation, and top-to-the-NW kinematics; C: during the E_{1b} event, the NW-SE shortening caused the folding of the foliation in the mylonitic zone and the orthogneiss, the formation of NE-SW folds. The Gneiss Unit thrusted on the Deformed Volcanic Rocks Unit, at depth migmatite developed; D: during the E_2 event, a NW-SE stretching regime dominated the Changle-Nan'ao belt in which a large amount of undeformed granitoids and NE-SW striking dykes emplaced.

Figure 12. Interpretative lithosphere-scale cross section of the East Asia Continental Margin during the Early Cretaceous. The Changle-Nan'ao Belt is interpreted as a magmatic arc back-thrusted to the NW in response to the continental subduction, and collision of the West Philippines microcontinent below the South China Block.

Table 1. AMS measurement data of the deformed volcanic rocks and orthogneiss

Lat: latitude, long: Longitude, lith: lithology, Km: mean magnetic susceptibility, P_J and T: corrected anisotropy degree and shape parameter, respectively, K_1 and K_3: magnetic lineation and pole of magnetic foliation, respectively, Inc: inclination, Dec: declination, α_{95}max and α_{95}min: long and short axis of ellipsoid uncertainty, respectively, DV, Deformed volcanic rocks, OG, Orthogneiss, Mig, Migmatite.

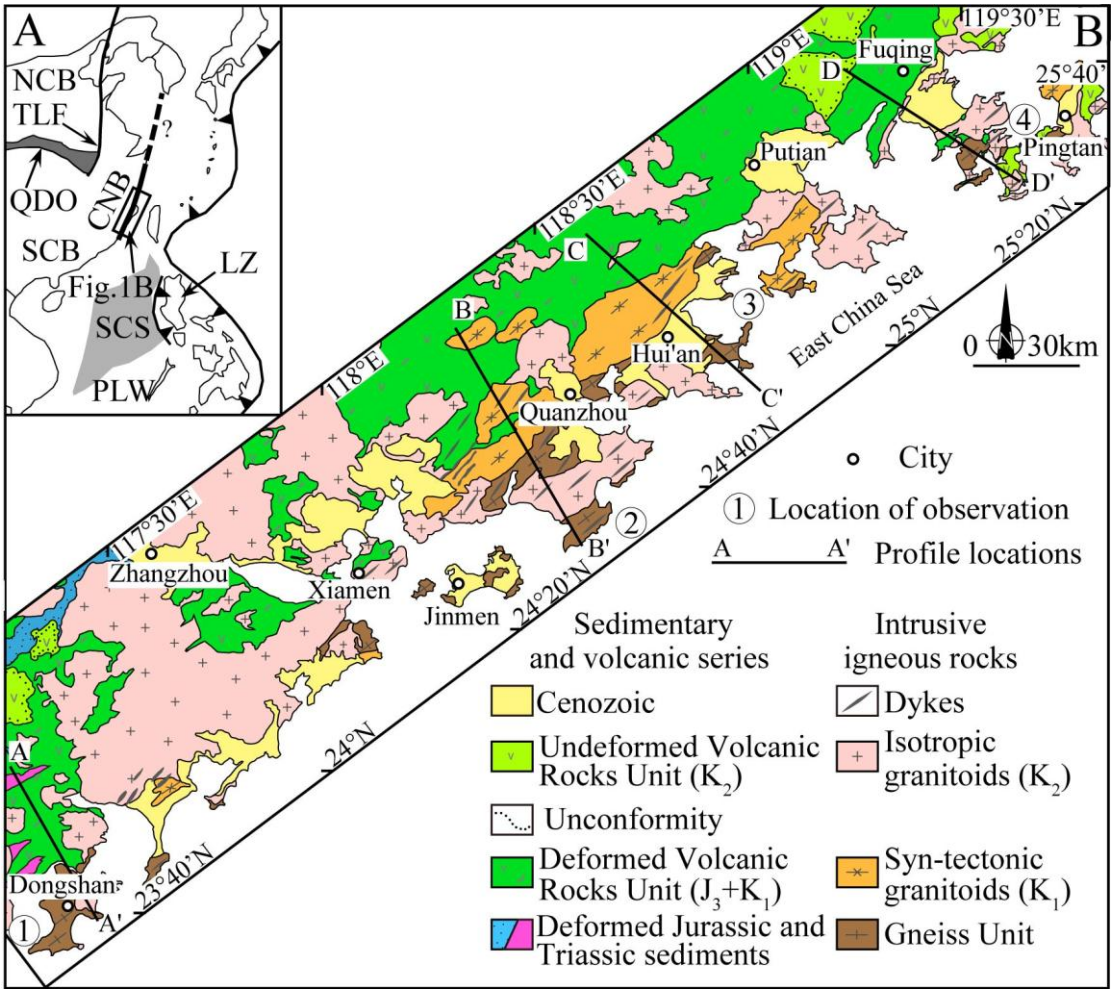

Figure 1. A: Sketch map of the present East Asia Continental Margin geodynamics. NCB: North China Block; TLF: Tan-Lu fault; QDO: Qinling-Dabie Orogen; SCB: South China Block; CNB: Changle-Nan'ao Belt; SCS: South China Sea; LZ: Luzon Island; PLW: Palawan Island. B: Sketch geologic map of the Changle-Nan'ao Belt.

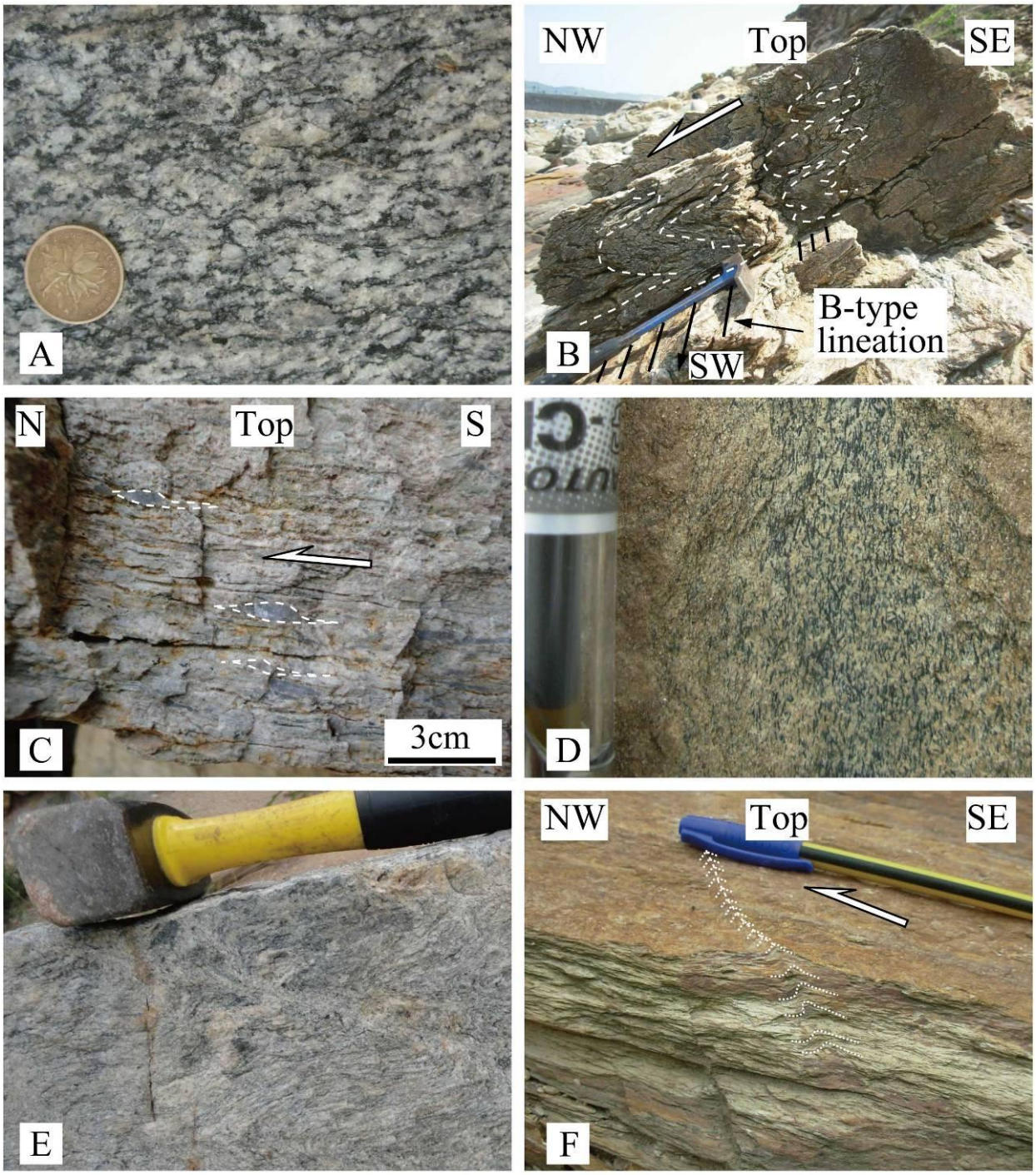
A
NW
Top
SE
B
B-type
lineation
SW
N
Top
S
C
3cm
D
E
NW
Top
SE
F

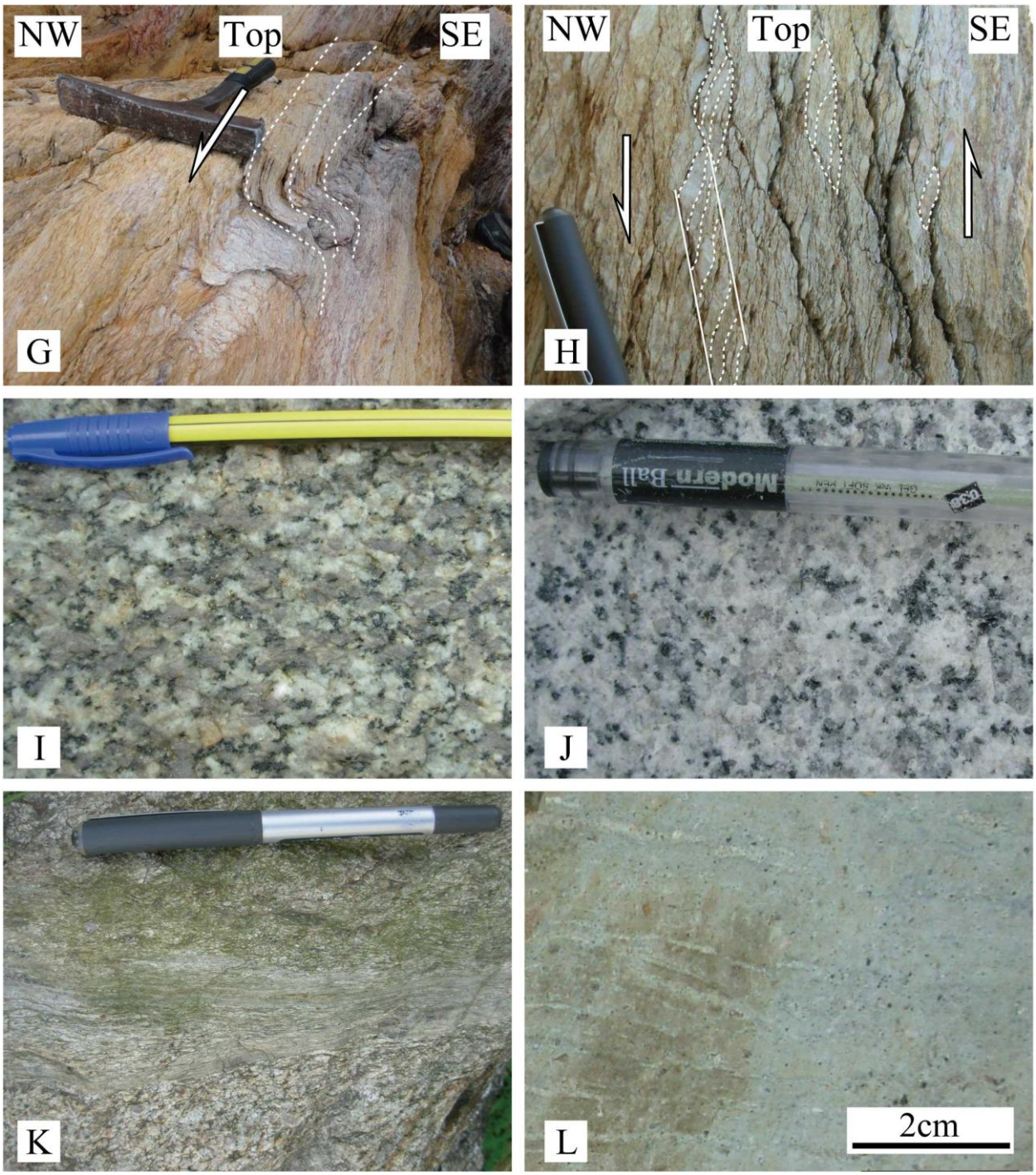

Figure 2. A: E_1 pervasively deformed granitoid (orthogneiss) in sub-solidus state (GPS: 25.45° N, 119.51° E); B: E_{1b} NW verging fold with NE-SW axis in the Dongshan island (GPS: 23.60° N, 117.43° E); C: E_{1a} mylonitic granitoid, section parallel to the lineation and perpendicular to the foliation (GPS: 23.74° N, 117.59° E); D: amphibole gneiss with down-dip lineation formed by oriented amphiboles (GPS: 24.63° N, 118.41° E); E: migmatite with folded foliation (GPS: 23.69° N, 117.34° E); F: mylonitic volcanic rocks with asymmetric kinks, section parallel to the lineation and perpendicular to the foliation (GPS: 24.96° N, 118.34° E); G: asymmetric fold of mylonitic volcanic rocks indicating NW-side-moving down and SE-side-moving up sense of shear, near the boundary between the Deformed Volcanic

Rocks Unit and the Gneiss Unit (GPS: 25.47° N, 119.44° E); H: shear bands of mylonitic volcanic rocks indicating a NW-side-moving down and SE-side-moving up sense of shear, near the boundary between the Deformed Volcanic Rocks Unit and the Gneiss Unit (GPS: 25.47° N, 119.44° E); I: Early Cretaceous syn-tectonic granitoid with oriented minerals near the boundary of the pluton with country rocks (GPS: 25.58° N, 119.69° E); J: Late Cretaceous granitoid with undeformed minerals (GPS: 24.64° N, 118.58° E); K: E_3 NE-SW striking cm-sized mylonitic shear zone crosscutting Late Cretaceous an undeformed isotropic granitoid (GPS: 25.40° N, 119.52° E); L: Undeformed Late Cretaceous volcanic rocks (GPS: 25.70° N, 119.29° E).

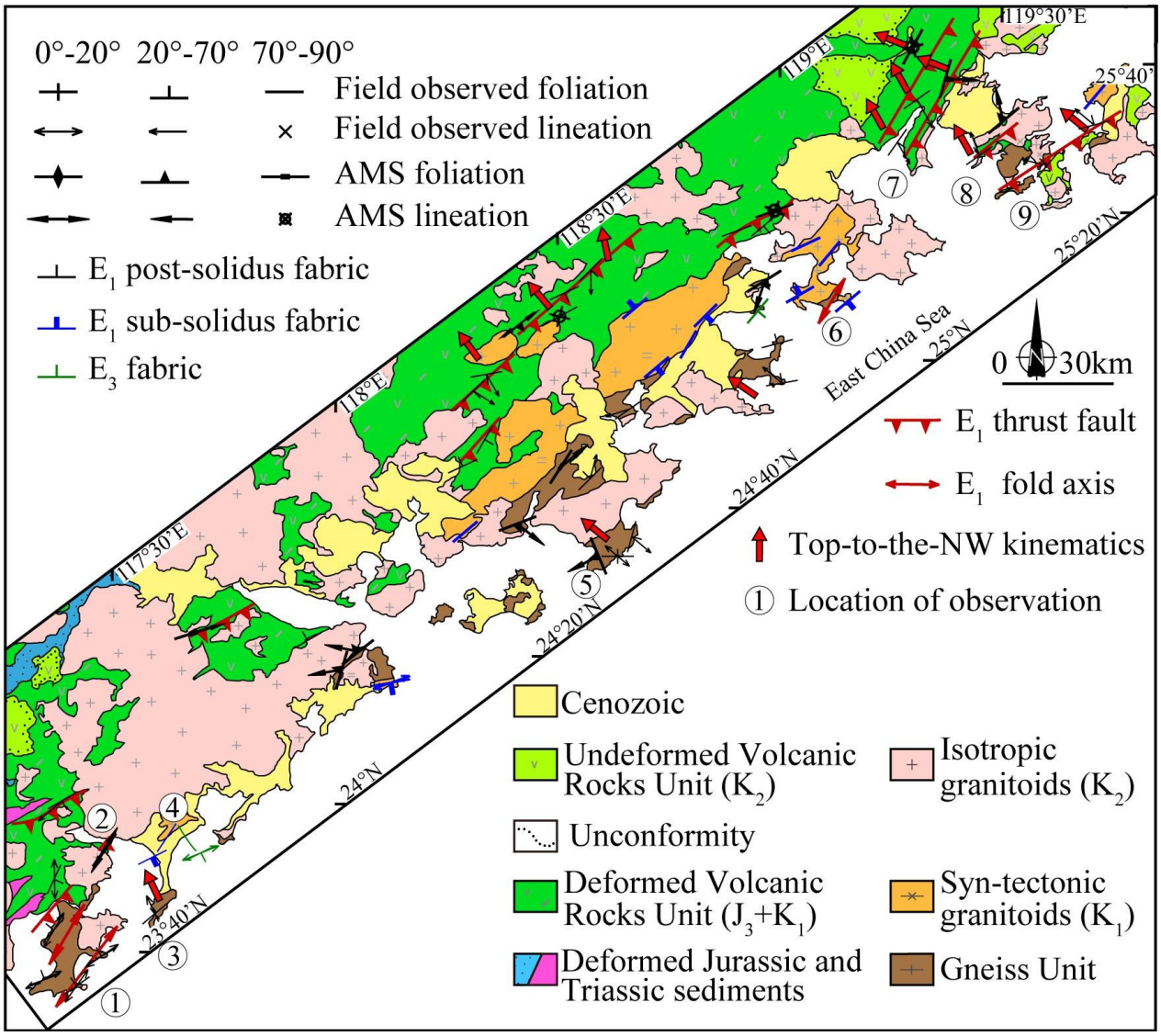

Figure 3. Representative field observed fabric and laboratory measured magnetic fabric of CNB and their structural interpretation. The dip of the foliation/magnetic foliation and the plunge of the lineation/magnetic lineation, please refer to Appendix 2.

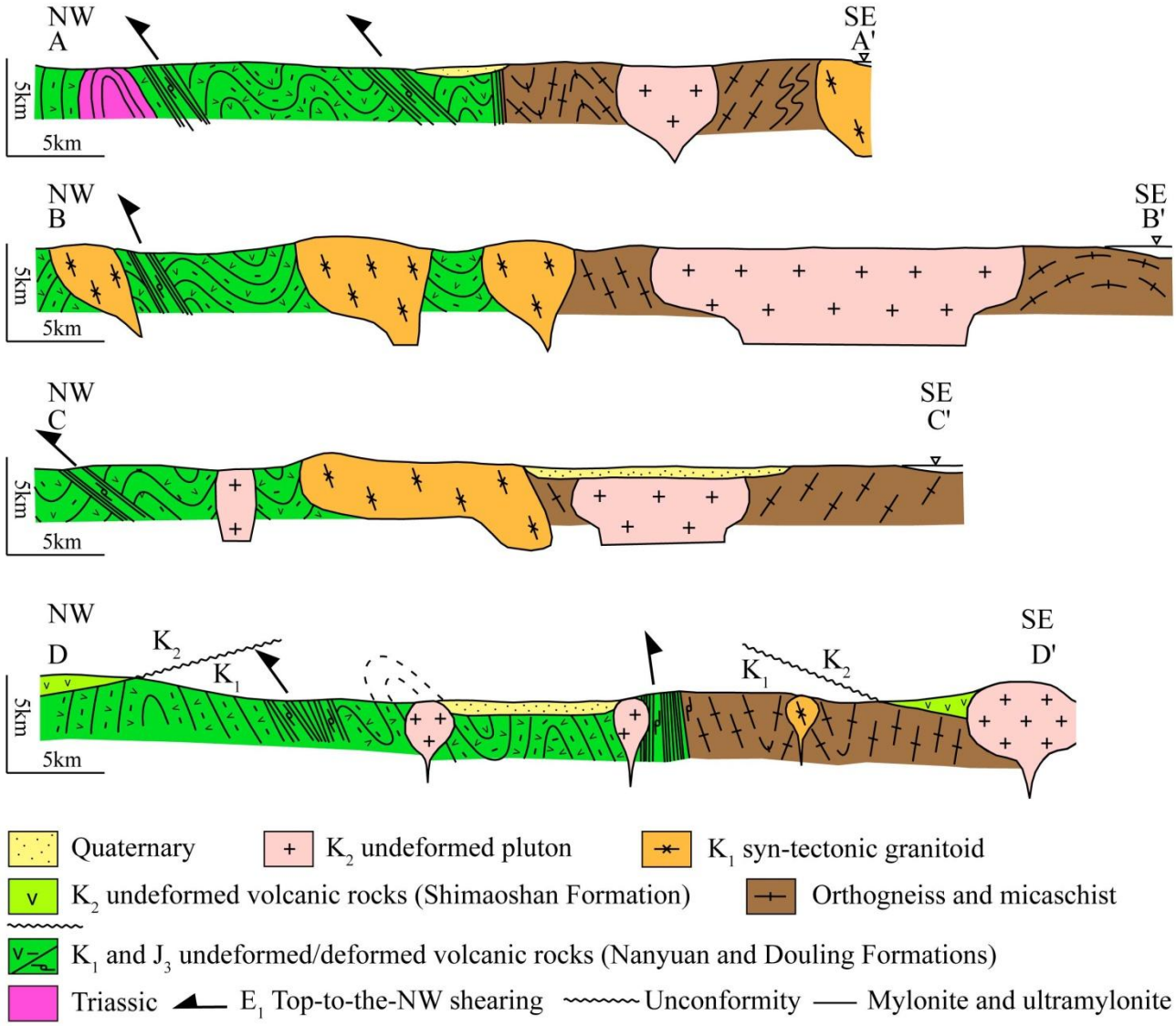

Figure 4. NW-SE representative cross sections illustrating the bulk architecture of the Changle-Nan'ao Belt. Profile locations refer to line AA', BB', CC' and DD' in Fig. 1B.

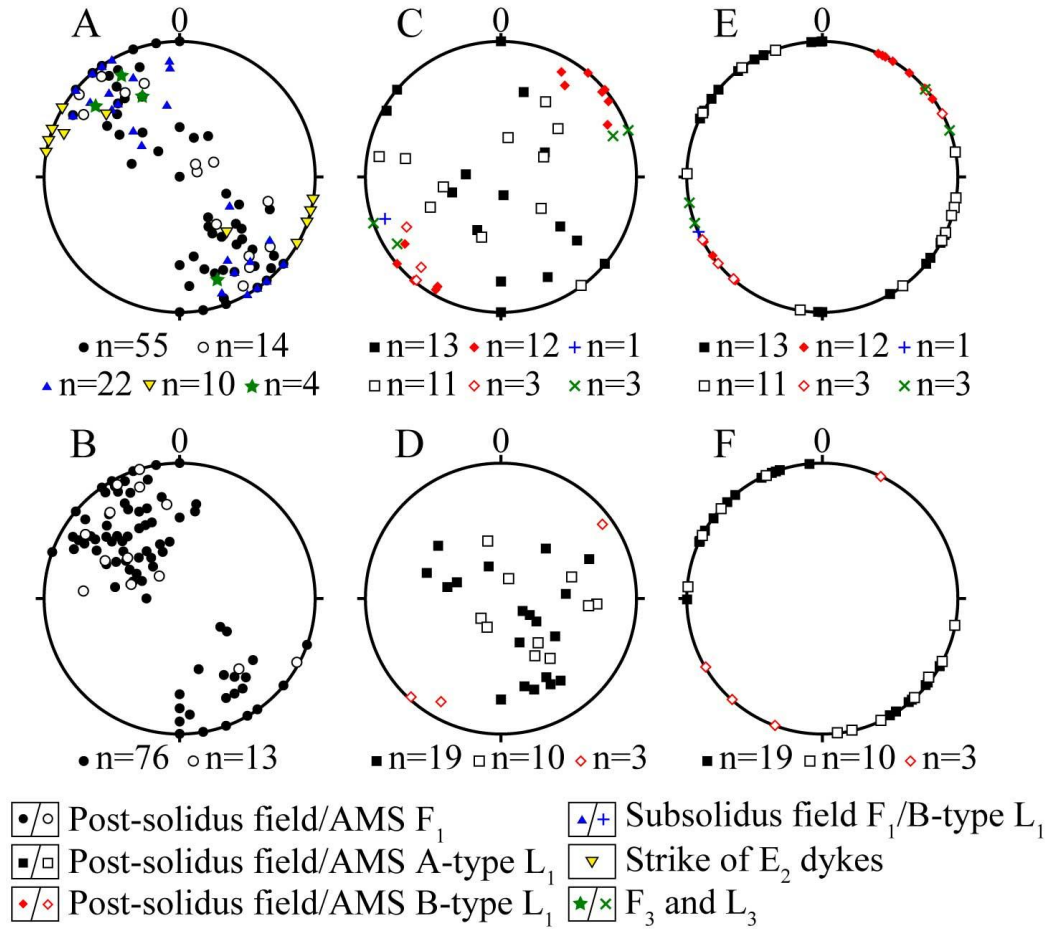

Figure 5. Equal-area lower hemisphere projections of total fabrics of the Changle-Nan'ao Belt. A: foliation pole of gneiss, syn-tectonic granitoid, E_3 shear zone, and strike of E_2 dykes; B: foliation pole of deformed volcanic rocks; C: lineation of E_1 gneiss, E_1 sub-solidus granitoid and E_3 narrow shear zone; D: lineation of deformed volcanic rocks; E: lineation of gneiss, E_1 sub- solidus granitoid and E_3 shear zone after correcting foliation to flat; F: lineation of deformed volcanic rocks after correcting foliation to flat. Solid and open circles/rectangles represent E_1 field and AMS foliation/A-type lineation. Solid and open diamonds represent E_1 field and AMS B-type lineation, Triangle and cross represent sub-solidus field foliation and B-type lineation, reverse triangle represents strike of E_2 dykes, Star and oblique cross represent E_3 foliation and lineation, respectively. The stereo projection of the AMS ellipsoid, please refer to Appendix 3.

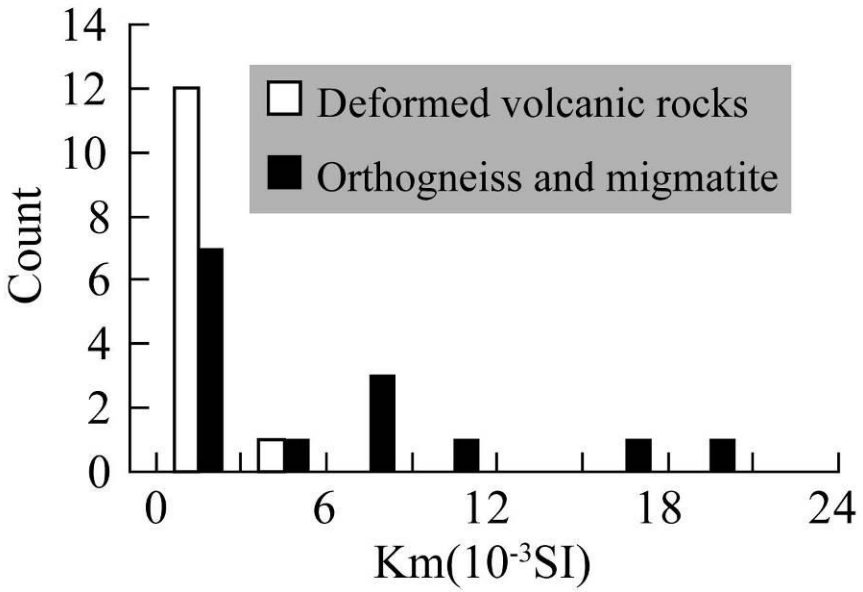

Figure 6. Distribution of the bulk magnetic susceptibility of magmatic rocks in the Changle-Nan'ao Belt.

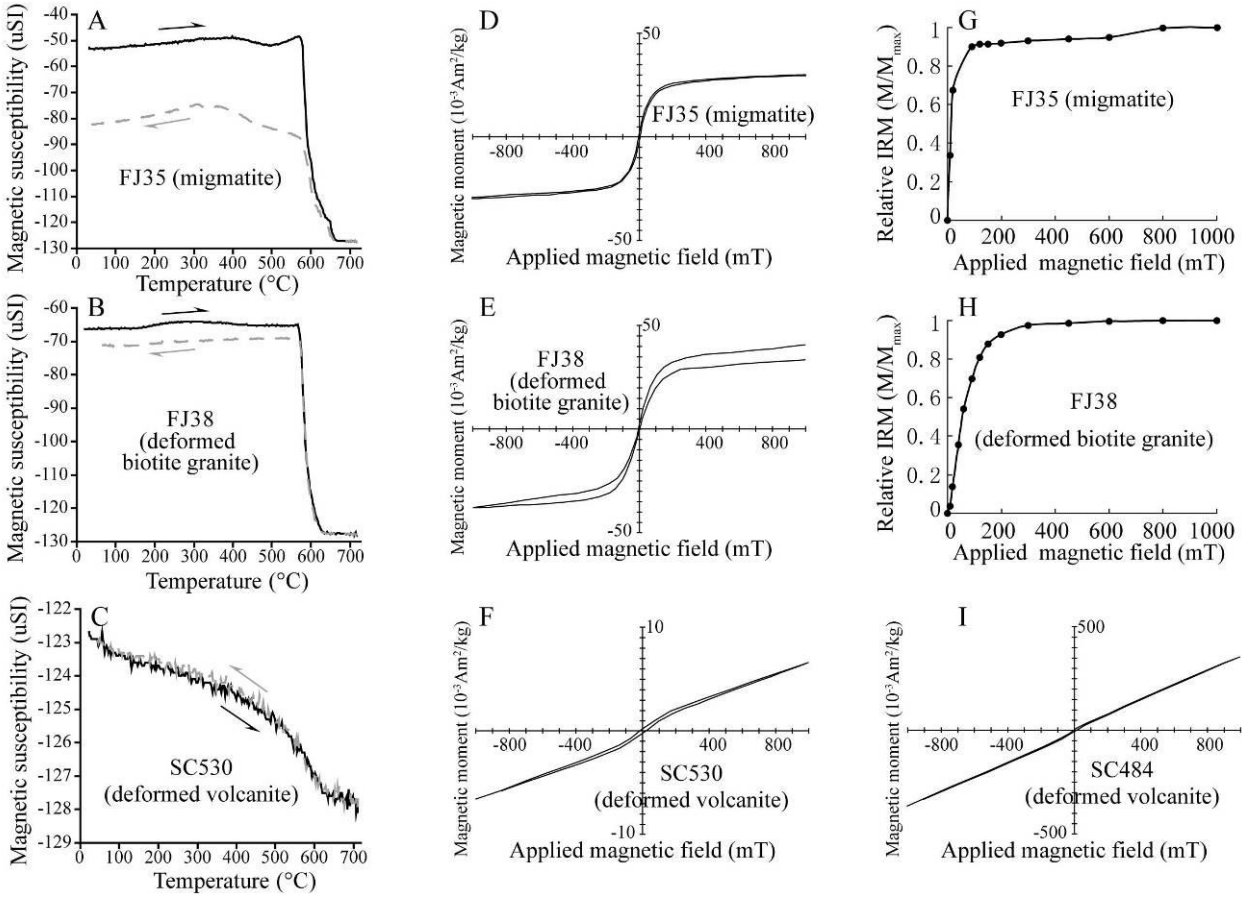

Figure 7, Thermal-Susceptibility, Isothermal Remanent Magnetization (IRM), Hysteresis Loop diagram of the deformed rocks of the Changle-Nan'ao Belt. The analyzed samples are located in Table 1.

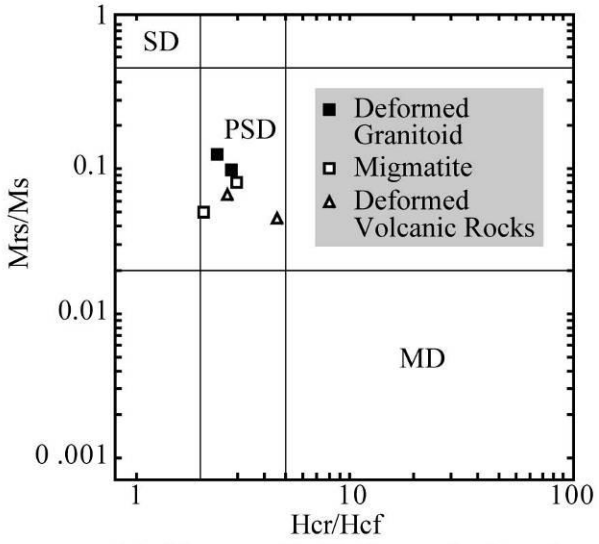

Mrs/Ms versus Hcr/Hc for samples from the Changle-Nan'ao Belt, with the boundaries of SD and MD behaviours for magnetite taken from the values of Dunlop (2002)

Figure 8. Day-plot diagram of measured samples of the Changle-Nan'ao Belt to define the magnetite size. Mrs: saturation remanence, Ms: saturation magnetization, Hcr: remanent coercive force Hcf: ordinary coercive force, SD: single domain, PSD: pseudo-single domain, MD: multi-domain.

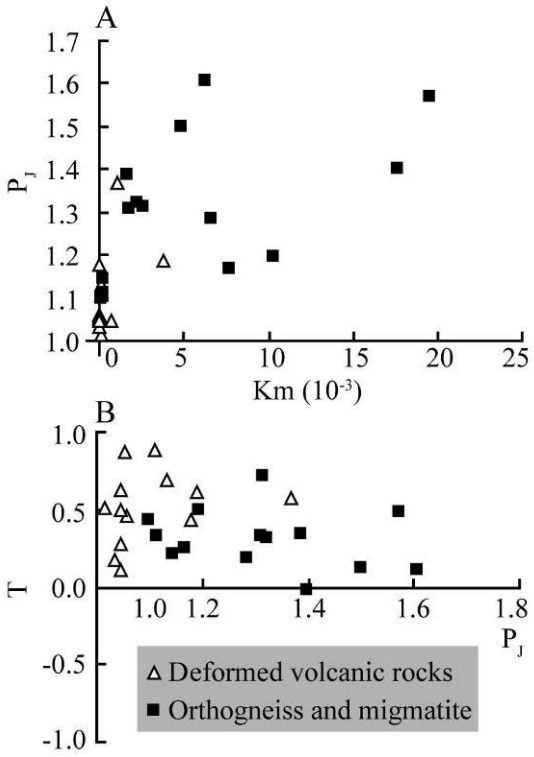

Figure 9. AMS scalar parameters for each site and main lithologies. A: P_J (corrected anisotropy degree) vs. Km (mean bulk magnetic susceptibility in 10^{-3} SI); B: T (shape parameter) vs. P_J (corrected anisotropy degree). The calculations of T and P_J can be found in Jelinek (1981).

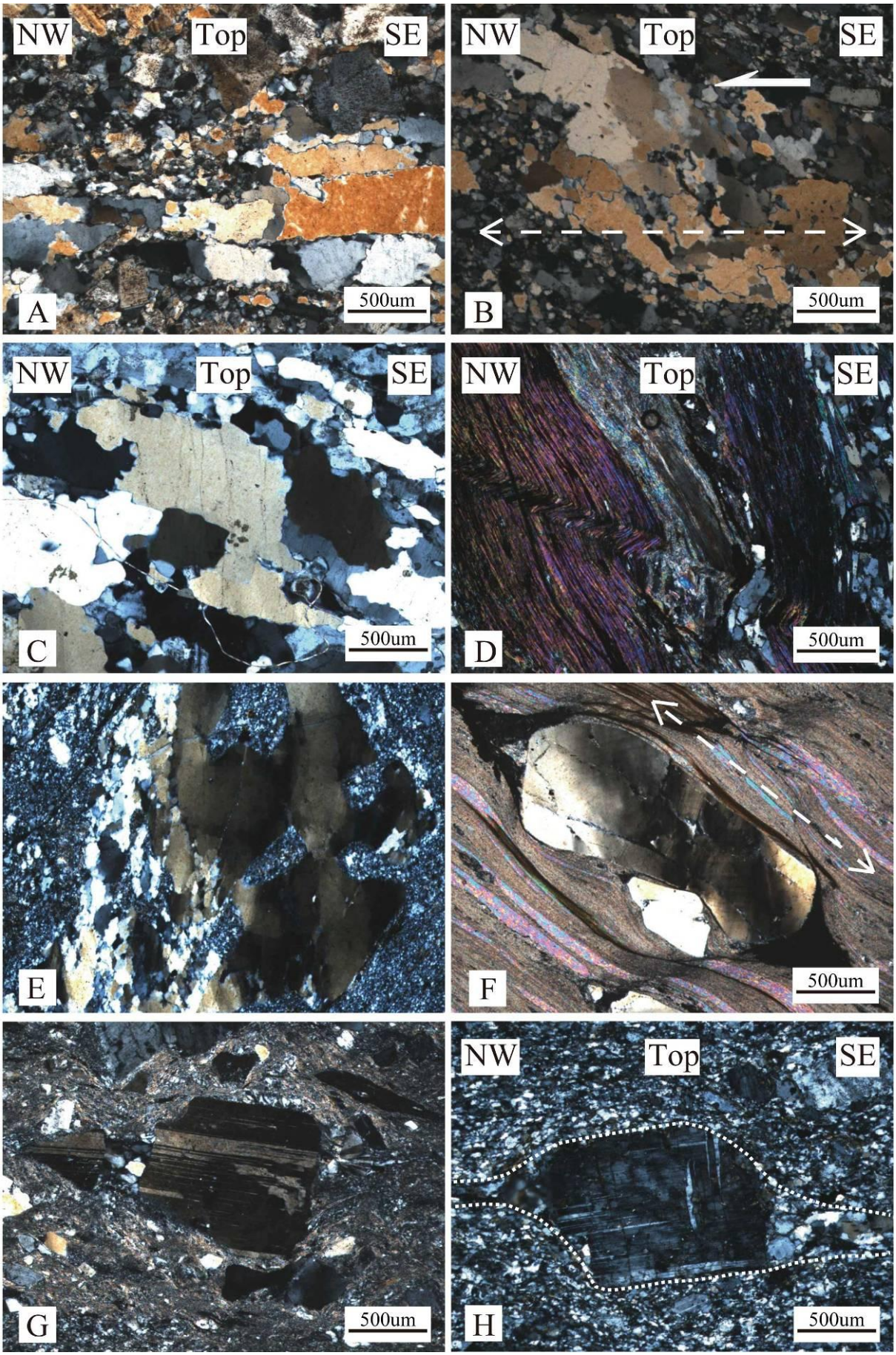
NW
Top
SE
A
500um
NW
Top
SE
B
500um
NW
Top
SE
C
500um
NW
Top
SE
D
500um
E
F
500um
G
500um
NW
Top
SE
H
500um

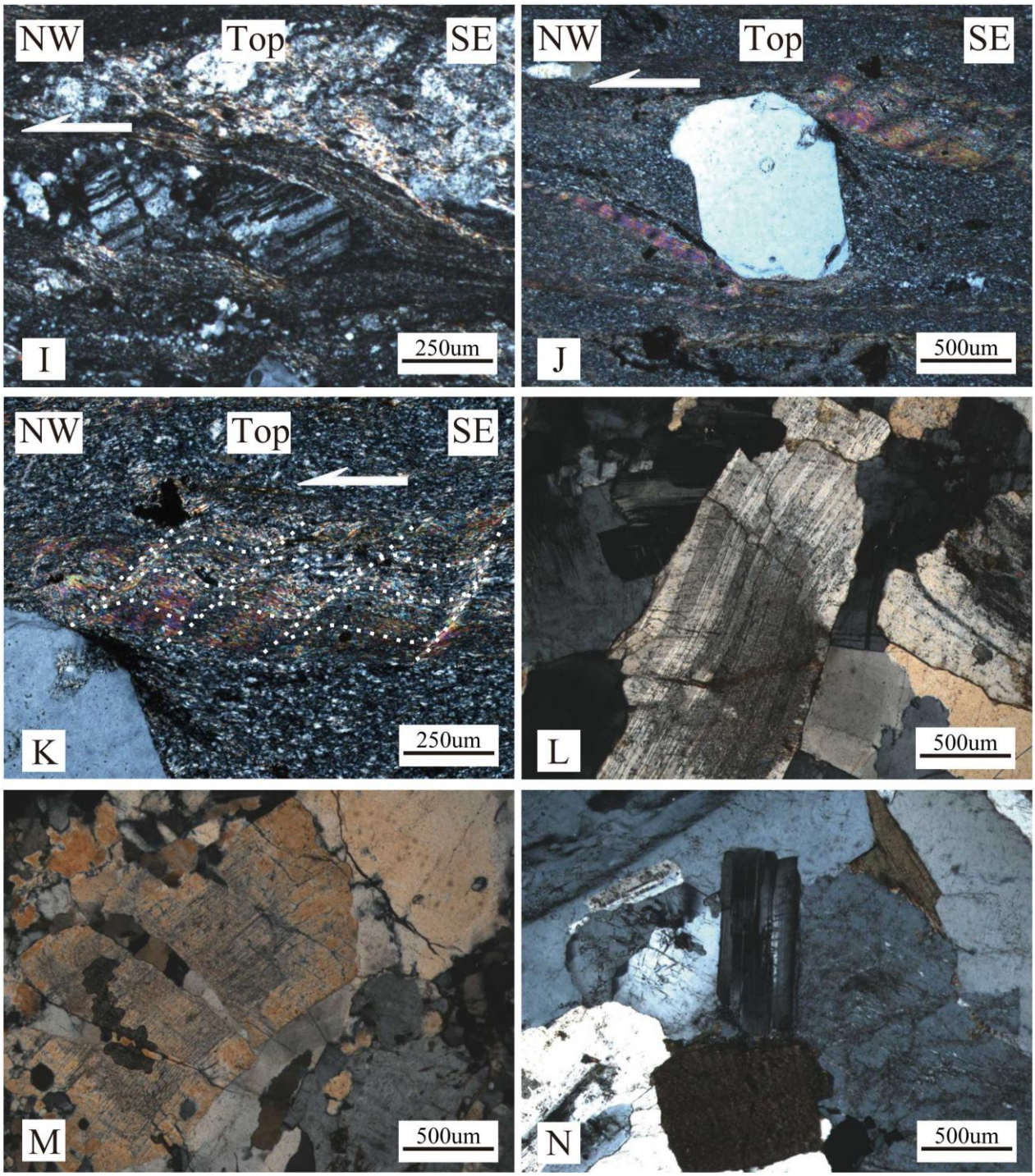

Figure 10. Microscopic photo of the rocks in the CNB. A: In the pervasively post-solidus deformed granitoid, quartz grains were stretched and plastically deformed (GPS: 23.74° N, 117.59° E); B: In the pervasively post-solidus deformed granitoid, stretched quartz grains experienced a dynamic recrystallization responsible for the development of an oblique shape fabric indicating a top-to-the-NW shear sense (GPS: 23.75° N, 117.60° E); C: In the pervasively post-solidus deformed granitoid, quartz grains were deformed with a sigmoidal shape indicating a top-to-the-NW shear sense (GPS: 23.76° N, 117.61° E); D: Kinked micas overturned to NW showing a NW-SE shortening (GPS: 23.60° N, 117.43° E); E: In the deformed volcanic rocks,

quartz was dynamic recrystallized, and newly formed tiny quartz neograins elongated parallel to the stretching lineation (marked by the dashed line) (GPS: 25.55° N, 119.35° E); F: In the deformed volcanic rocks, quartz develops pressure shadow, and mica is stretched parallel to the lineation (GPS: 24.96° N, 118.34° E); G: In the deformed volcanic rocks, plagioclase was cracked and boudinaged (GPS: 25.62° N, 119.36° E); H: In the deformed volcanic rocks, asymmetric pressure shadow indicates a top-to-the NW shear sense (GPS: 25.53° N, 119.71° E); I: In the deformed volcanic rocks, the plagioclase is cracked and developed domino structure indicating a top-to-the-NW shear sense (GPS: 25.20° N, 118.58° E); J: In the deformed volcanic rocks, quartz with mica tails indicating a top-to-the-NW shear sense (GPS: 25.59° N, 119.31° E); K: In the deformed volcanic rocks, shear band indicates a top-to-the-NW shear sense (GPS: 25.59° N, 119.31° E); L: At the margin of syn-tectonic granitoid pluton, plagioclase was bent and cracked; the cracks do not penetrate into the granite matrix (GPS: 24.89° N, 118.45° E); M: At the margin of syn-tectonic granitoid pluton, cracked plagioclase infilled with quartz (GPS: 24.91° N, 118.45° E); N: The isotropic granitoids exhibit a magmatic texture with no deformed minerals (GPS: 23.85° N, 117.48° E).

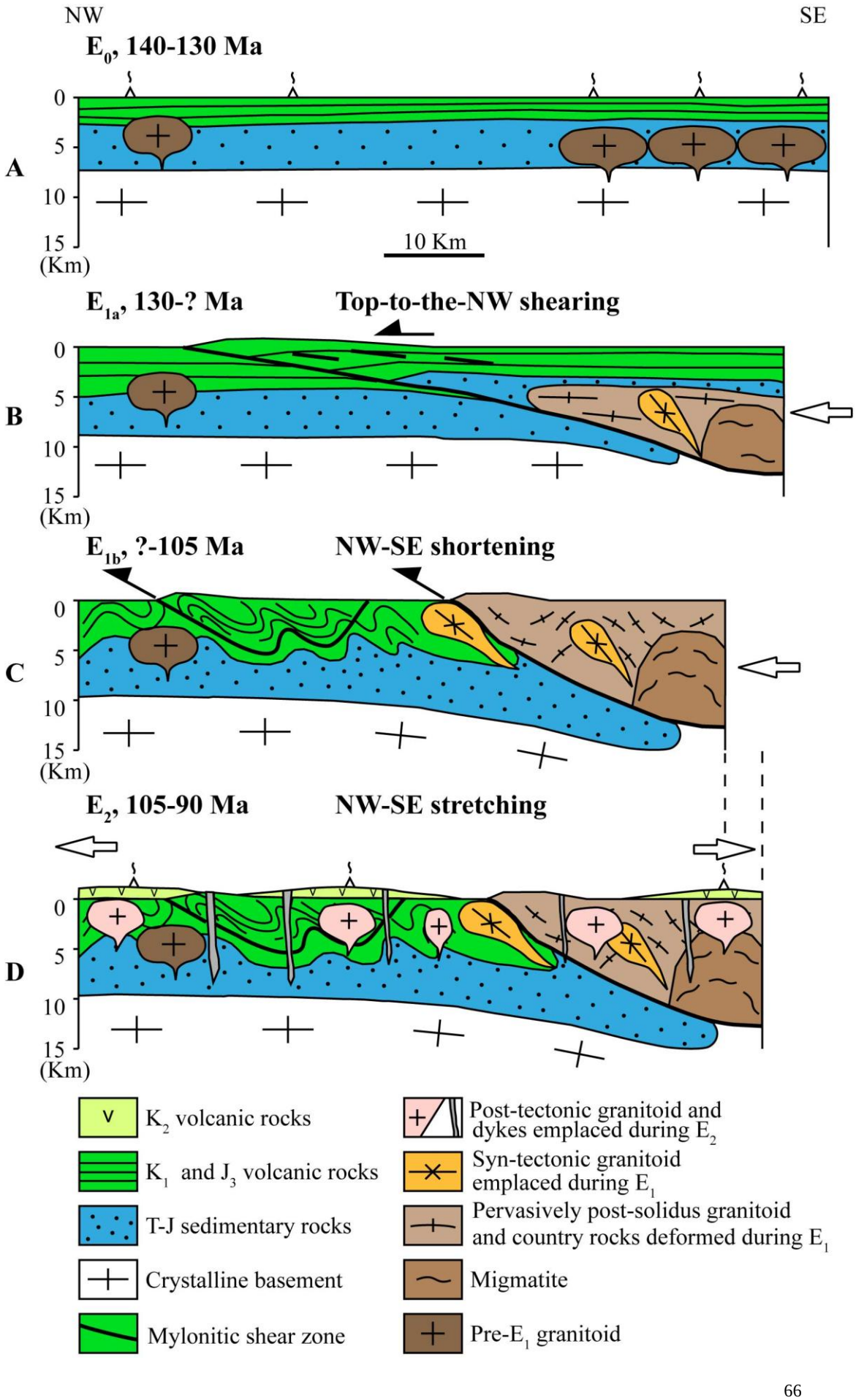
NW
SE
E0, 140-130 Ma
A
0
5
10
15
(Km)
10 Km
E1a, 130-? Ma
Top-to-the-NW shearing
B
E1b, ?-105 Ma
NW-SE shortening
C
E2, 105-90 Ma
NW-SE stretching
D
K2 volcanic rocks
K1 and J3 volcanic rocks
T-J sedimentary rocks
Crystalline basement
Mylonitic shear zone
Post-tectonic granitoid and dykes emplaced during E2
Syn-tectonic granitoid emplaced during E1
Pervasively post-solidus granitoid and country rocks deformed during E1
Migmatite
Pre-E1 granitoid

Figure 11. Crustal-scale structural evolution model of the Changle-Nan'ao Belt during the Cretaceous. A: at ca. 140-130 Ma, voluminous magmatism represented by extensive volcanism and plutonism throughout the belt; B: during the E_{1a} event starting at ca. 130 Ma, the belt experienced a top-to-the-NW shearing event characterized by the development of weakly inclined mylonitic zones in the Deformed Volcanic Rocks Unit, and pervasive post solidus deformation in the Gneiss Unit. In both units, the ductile shearing is represented by a NW-SE stretching lineation, and top-to-the-NW kinematics; C: during the E_{1b} event, the NW-SE shortening caused the folding of the foliation in the mylonitic zone and the orthogneiss, the formation of NE-SW folds. The Gneiss Unit thrusted on the Deformed Volcanic Rocks Unit, at depth migmatite developed; D: during the E_2 event, a NW-SE stretching regime dominated the Changle-Nan'ao belt in which a large amount of undeformed granitoids and NE-SW striking dykes emplaced.

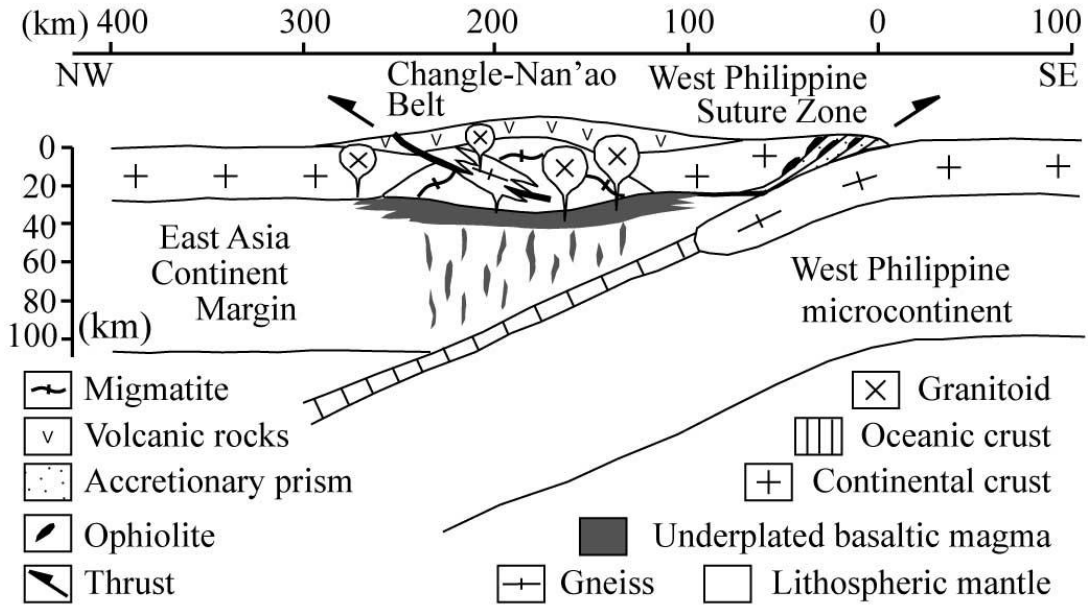

Figure 12. Interpretative lithosphere-scale cross section of the East Asia Continental Margin during the Early Cretaceous. The Changle-Nan'ao Belt is interpreted as a magmatic arc back-thrusted to the NW in response to the continental subduction, and collision of the West Philippines microcontinent below the South China Block.

Table 1. AMS measurement data of the deformed volcanic rocks and orthogneiss

site	Coordinates		Lith	n	Km	P_J	T	K_1				K_3			
	Long (°E)	Lat (°N)			(10^{-4}SI)			Dec (^{o})	Inc (^{o})	α_{95max} (^{o})	α_{95min} (^{o})	Dec (^{o})	Inc (^{o})	α_{95max} (^{o})	α_{95min} (^{o})
FJ28	24.63	118.41	OG	10	10300	1.194	0.503	128.3	59.1	21.1	9.5	339.2	27.2	13.6	6.9
FJ35	24.56	118.60	Mig	11	6610	1.286	0.189	241.9	22.2	39	8.9	66.8	67.7	16.5	9.9
FJ37	24.57	118.62	Mig	8	7660	1.166	0.246	279.4	9.8	15.9	9.8	74.2	79.1	22.3	5
FJ38	24.56	118.64	OG	5	6210	1.605	0.116	143.6	0.4	11.2	3.4	51.8	77.9	16.3	3.3
FJ41	24.89	118.66	OG	10	17700	1.4	-0.014	246.7	42.7	6.3	2.3	149.8	7.5	8.4	4.6
FJ49	25.45	119.51	OG	8	1810	1.31	0.328	65	61.6	10.5	5	322.1	6.9	8.9	3
FJ50	25.44	119.53	OG	6	4900	1.5	0.119	10.3	66	7.4	2.2	142.4	16.6	5.1	3.7
FJ51	25.37	119.49	OG	7	140	1.1	0.427	30.8	35.8	10.5	4	138.8	23.2	11.1	5.2
FJ55	25.18	118.97	Mig	10	19500	1.571	0.483	197.7	51.3	7.4	4.8	327	26.9	9.2	5
FJ76	23.69	117.34	Mig	8	185	1.143	0.213	221.4	11.9	29.2	8.3	127.8	16.7	33.8	14.1
FJ85	24.34	118.05	OG	6	204	1.114	0.325	280.7	29	12.2	3.7	142.4	53.4	5.2	3.7
FJ86	24.31	118.01	OG	6	2250	1.323	0.314	260	54.5	19.7	8.7	105.6	32.7	17.8	7.6
SC435	24.76	118.51	OG	9	2570	1.314	0.714	49.9	44.2	3.7	1	302.9	16.7	2.7	1.5
SC458	25.54	119.25	DV	11	9.5	1.179	0.433	222.4	1.7	23.7	3.9	317.8	71.9	15.2	5.0
SC484	25.71	119.30	DV	7	51.8	1.014	0.512	21.2	77.3	32.4	4.2	118.6	1.7	9.8	6.2
SC487	25.64	119.31	DV	5	29.0	1.047	0.114	140.1	54.9	9.6	3.9	352.2	30.7	4.6	3.8
SC500	25.58	119.28	DV	6	6.0	1.033	0.171	149.5	49.3	15.6	6.4	274.4	29.5	79.1	5.3
SC506	25.49	119.27	DV	6	36.3	1.053	0.871	140.7	42.3	43.7	1.7	307.2	46.9	3.6	0.9
SC509	25.49	119.30	DV	7	39.7	1.131	0.689	94.8	35.4	10.8	3.4	308.0	49.7	4.4	0.9
SC513	25.62	119.36	DV	9	29.7	1.057	0.457	93.3	29.8	3.1	2.7	286.1	59.5	4.6	2.1
SC517	25.54	119.50	DV	7	3750.0	1.189	0.610	347.1	54.2	5.4	2.6	139.9	32.6	3.0	1.6
SC530	25.33	118.96	DV	14	38.0	1.045	0.279	205.7	70.8	4.0	1.6	340.3	13.7	4.0	1.6
SC551	25.10	118.51	DV	8	52.9	1.109	0.885	225.3	73.1	10.7	2.0	331.3	4.8	2.2	1.4
SC560	25.09	118.43	DV	6	37.7	1.046	0.620	53.8	8.0	7.9	2.2	321.0	19.4	4.2	1.8
SC595	23.90	117.48	DV	8	1050.0	1.367	0.570	210.1	12.9	9.6	4.7	304.2	17.1	5.5	2.5
SC659	23.72	117.40	OG	8	1600	1.388	0.338	219.2	1.6	9.0	2.7	309.3	4.8	7.6	2.5
SC668	24.39	117.70	DV	5	705.0	1.046	0.493	73.0	44.7	8.4	0.5	342.7	0.3	4.8	0.5

Lat: latitude, long: Longitude, lith: lithology, Km: mean magnetic susceptibility, P_J and T: corrected anisotropy degree and shape parameter, respectively, K_1 and K_3: magnetic lineation and pole of magnetic foliation, respectively, Inc: inclination, Dec: declination, α_{95}max and α_{95}min: long and short axis of ellipsoid uncertainty, respectively, DV, Deformed volcanite, OG, Orthogneiss (pervasively ductile deformed granitoids), Mig, Migmatite.

Highlights

►This work conducts a systematic structural and AMS investigation on CNB.
►This work interprets the CNB as a NW-directed thrust belt between 130-105Ma.
►The CNB was a back thrust belt due to the collision between west Philippines and SCB.